Upgrade of Atmospheric Motion Vector Derivation Algorithms at JMA/MSC

OYAMA Ryo[1]

Abstract

The Meteorological Satellite Center (MSC) of the Japan Meteorological Agency (JMA) has been producing Atmospheric Motion Vectors (AMV) by using the successive images of geostationary satellites since 1978. At present, JMA/MSC generates four types of AMVs, IR AMVs, WV AMVs, VIS AMVs and SWIR AMVs, which are derived from Infrared (IR: 10.8 μm), Water Vapor (WV: 6.8 μm), Visible (VIS: 0.63 μm) and Short-wave Infrared (SWIR: 3.8 μm) images of MTSAT-1R. The AMV data is important observational wind data for Numerical Weather Prediction (NWP). Hence, the data is used as assimilation data in the NWP models of JMA, and foreign numerical prediction centers, such as the European Centre for Medium-Range Weather Forecasts (ECMWF), United Kingdom Meteorological Office (UKMO), National Oceanic and Atmospheric Administration (NOAA)/ National Centers for Environmental Prediction (NCEP) and so forth.

This paper describes the new AMV derivation schemes introduced in the upgrade at 05UTC on 19 May 2009 as well as reviews all of the current AMV derivation algorithms. The algorithms were upgraded in three ways. The first upgrade was of a height assignment scheme for high- and middle-level IR AMVs, which is linked to the cloud-tracking process. This upgrade led to improvements of the AMV quality, particularly, reduction of fast wind speed bias at middle level and increase of AMV at high level. Second, the optimum resizing of image segments for tracking clouds/water vapor patterns mitigated the large slow wind speed bias of high level IR and WV AMVs in winter hemispheres compared to the previous AMVs. Third, the derivation area was expanded from 50S-50N and 90E-170W to 60S-60N and 90E-170W, which led to the possibility of providing AMV data for higher latitude for users. The current algorithms are applied to the ongoing AMV reprocess for GMS-1, -3, -4 and -5, and GOES-9 and MTSAT-1R at JMA/MSC. The reprocessed AMVs will be provided for the Japanese 55-year Reanalysis (JRA-55) which is scheduled for between 2009 and 2012, and the Sustained, Coordinated Processing of Environmental Satellite Data for Climate Monitoring (SCOPE-CM).

1. Introduction

The Meteorological Satellite Center (MSC) of the Japan Meteorological Agency (JMA) has been producing Atmospheric Motion Vectors (AMV) products from the satellite images of GMS -1 to 5, GOES-9, and MTSAT-1R since April 1978. The AMV data is important observational wind data as an assimilation data in Numerical Weather Prediction (NWP). In computing AMV, first an atmospheric movement vector is derived by tracking clouds and/or water vapor patterns. Then, the vector is assigned to a specific height level estimated using the brightness temperature of Infrared images in addition to referring to NWP forecast fields. The data is used in the NWP models of JMA and foreign numerical prediction centers, such as the European Centre for Medium-Range Weather Forecasts (ECMWF), United Kingdom Meteorological Office (UKMO), National Oceanic and Atmospheric Administration (NOAA)/ National Centers for Environmental Prediction (NCEP) and so forth.

[1]System Engineering Division, Data Processing Department, Meteorological Satellite Center

（Received May 22, 2009, Accepted November 9, 2009）

JMA/MSC generates four types of AMVs, i.e., IR AMVs, VIS AMVs, WV AMVs and SWIR AMVs from three successive images of MTSAT-1R. Table 1 shows an outline of JMA's operational AMVs. The motion vectors for IR AMVs, VIS AMVs, WV AMVs and SWIR AMVs are derived using Infrared (IR: 10.8 μm), Visible (VIS: 0.63 μm), Water Vapor (WV: 6.8 μm) and Short-wave Infrared (SWIR: 3.8 μm) images, respectively. IR AMVs and VIS AMVs have been generated since April 1978 (Hamada, 1979). The generation of WV AMVs started in June 1995 with the introduction of a WV channel sensor mounted on GMS-5 (Uchida and Takata, 1996). Moreover, in accordance with the introduction of a SWIR channel sensor to MTSAT-1R, JMA/MSC started to derive SWIR AMVs as nighttime low-level winds using SWIR images at 07UTC on 25 March 2008 (Oyama and Shimoji, 2008). At present, JMA/MSC disseminates AMVs for the Northern Hemisphere at 00, 03, 06, 09, 12, 15, 18 and 21UTC and AMVs for the Southern Hemisphere at 00, 06, 12 and 18UTC to users in Binary Universal Form for data Representation (BUFR) via the Global Telecommunication System (GTS).

In recent years, JMA/MSC has performed some upgrades on AMV derivation to improve the quality of AMVs. At 06UTC on 30 May 2007, JMA/MSC introduced two upgrades (JMA, 2007; Imai and Oyama, 2008). One is an upgrade of the height assignment scheme for high- and middle-level IR AMVs and cloudy-region WV AMVs to mitigate the slow wind speed bias over high and middle latitudes. The other is the introduction of a scheme that optimizes the position of image segments which is used for tracking clouds/water vapor patterns using entropy. Furthermore, JMA started to use NWP-model Grid Point Values (GPVs) with higher temporal and spatial resolutions as reference data in computing AMVs at 05UTC on 9 October 2008 (JMA, 2009). The GPVs are generated from JMA's Global Spectral Model (GSM) first-guess fields which are forecasted at 00, 06, 12 and 18UTC (00 and 12UTC before the upgrade), and the spatial resolution of the GPV is 0.5 and 1.0 degree (1.25 and 2.5 degrees before the upgrade) latitude/longitude. The latest upgrade conducted at 05UTC on 19 May 2009 consists of an upgrade and an optimization of the AMV derivation schemes, and expansion of AMV derivation area. The purpose of this upgrade was to improve some erroneous height assignments in IR AMVs. To do so a height assignment scheme linked to the feature-tracking (i.e., cloud tracking) process was introduced. The optimization was to fix the large slow wind speed bias remaining in the previous high-level AMVs for winter hemispheres. This was accomplished by resizing the image segment for tracking clouds/water vapor patterns. In addition, the AMV derivation area was expanded from 50S-50N and 90E-170W to 60S-60N and 90E-170W.

This paper describes the new AMV derivation schemes introduced in the upgrade at 05UTC on 19 May 2009, and reviews all of the AMV derivation algorithms. Besides being applied to the operational AMVs, the new algorithms are also applied to the AMV reprocess for GMS-1, -3, -4 and -5, and GOES-9 and MTSAT-1R at JMA/MSC. The reprocessed AMVs will be provided for the second JMA reanalysis project (the Japanese 55-year Reanalysis: JRA-55) which is scheduled for between 2009 and 2012, and the Sustained, Coordinated Processing of Environmental Satellite Data for Climate Monitoring (SCOPE-CM).

The derivation algorithms are summarized focusing on the new schemes introduced at 05UTC on 19 May 2009 in Section 2. In Section 3, the improvements in AMV quality by introducing the new schemes are described. Finally, discussions and future plans on the development of JMA's AMVs are shown in Section 4.

2. Descriptions of AMV derivation algorithms

This section describes the AMV derivation algorithms

Table 1: MTSAT-1R AMVs generated by JMA/MSC

AMV type	Level of height *1	Time (UTC)	Image sector	Image interval (minutes)	Distribution
Infrared: IR (10.8 micrometer)	High, middle, low	00, 06, 12, 18	Northern and Southern Hemispheres	15	BUFR via GTS
		02-05, 08-11, 14-17, 20-23	Northern Hemisphere	30	03, 09, 15 and 21UTC: BUFR via GTS Other times: Internal use only
		01, 07, 13, 19	Northern Hemisphere	60	Internal use only
Water Vapor: WV (6.8 micrometer)	High, middle	00, 06, 12, 18	Northern and Southern Hemispheres	15	BUFR via GTS
		02-05, 08-11, 14-17, 20-23	Northern Hemisphere	30	03, 09, 15 and 21UTC: BUFR via GTS Other times: Internal use only
		01, 07, 13, 19	Northern Hemisphere	60	Internal use only
Visible: VIS (0.63 micrometer)	Low	00, 06	Northern and Southern Hemispheres	15	BUFR via GTS
		02-05, 08, 09, 21-23	Northern Hemisphere	30	03, 09 and 21UTC: BUFR via GTS Other times: Internal use only
		01, 07	Northern Hemisphere	60	Internal use only
Short-wave Infrared: SWIR (3.8 micrometer)	Low	12, 18	Northern and Southern Hemispheres	15	Internal use only
		08-11, 14-17, 20-23	Northern Hemisphere	30	Internal use only
		07, 13, 19	Northern Hemisphere	60	Internal use only

*1 High: above 400 hPa level, middle: 400-700 hPa level, and low: below 700 hPa level

which are used at JMA/MSC. Figure 1 shows the flow chart for the derivation processes. AMV derivations are performed in the respective flows for (a) Low-level AMVs (Low-level (below 700 hPa level) IR AMVs, VIS AMVs and SWIR AMVs), (b) High- (above 400 hPa level) and middle- (400-700 hPa level) level IR AMVs and (c) WV AMVs. The AMV derivation algorithm is basically composed of four processes, they are Target selection, Derivation of vectors by cross correlation matching (referred to as "Feature tracking"), Height assignment, and Automatic quality controls by the Quality Indicator (QI) and the Recursive Filter Function (RFF) quality flag. Target selection selects an appropriate cloud from an IR image or a water vapor pattern from a WV image that is used as the target to derive a motion vector in the Feature tracking process. Feature tracking is conducted to track the selected cloud and/or water vapor pattern and then derive a motion vector. In Height assignment, a specific height level is computed and given to each target with a motion vector.

Figure 2 shows the input data that are required for the AMV derivations. JMA/MSC uses three successive images (referred to as A, B, and C images) of IR, WV, VIS and SWIR. In addition to the image data, the Clear Sky Radiance (CSR) product is used. GPV data from JMA's Global Spectral Model (GSM) first-guess fields, i.e., the vertical temperature profile which is corrected to take account of the atmospheric attenuation effect (VTP), the simulated IR and WV radiances from ideal opaque clouds (IRWV_TBL) at each pressure level, and the wind field (GPV_WIND) are used in the AMV derivations as reference forecast data.

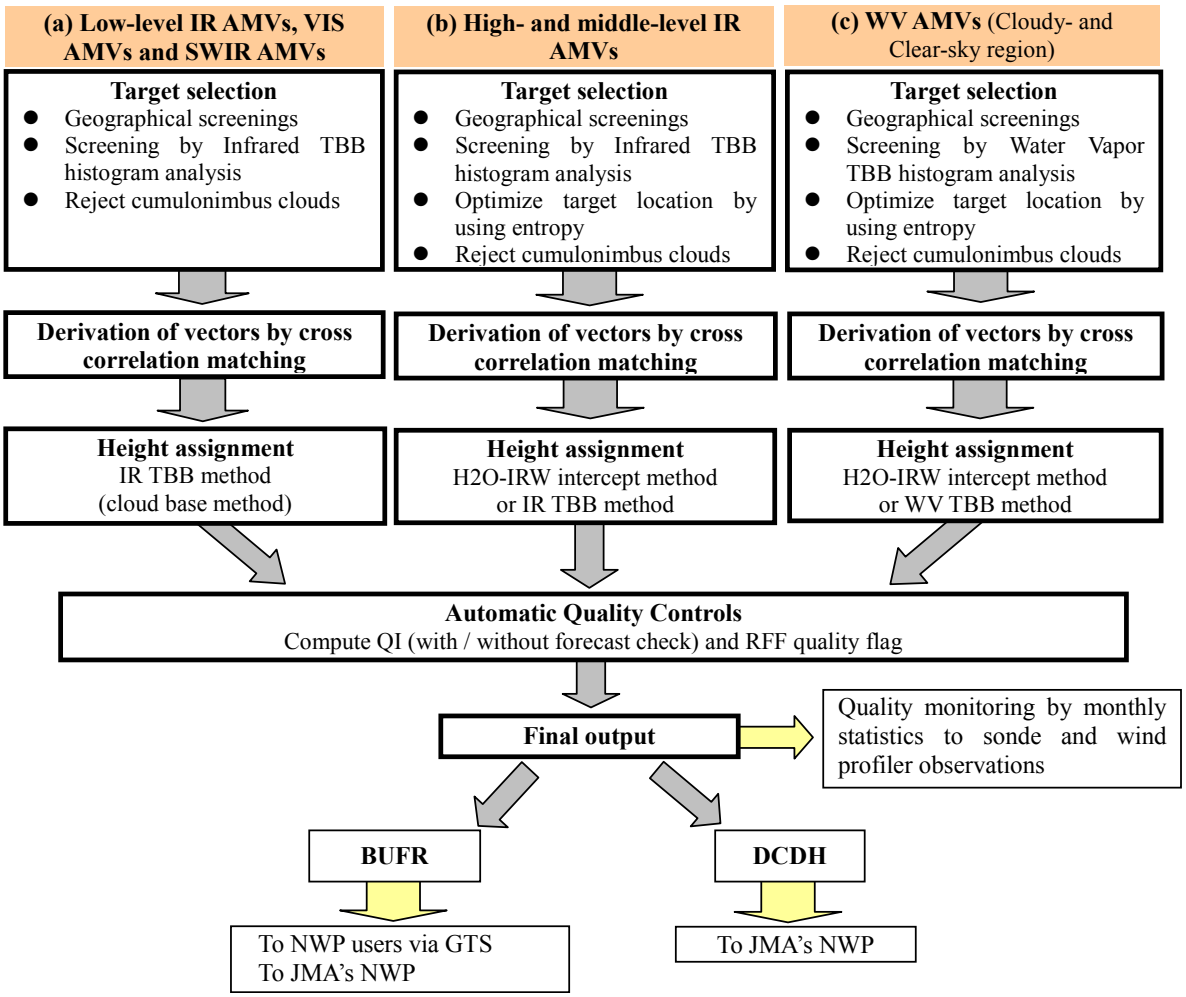

Figure 1: Flow chart on AMV derivation at JMA/MSC.

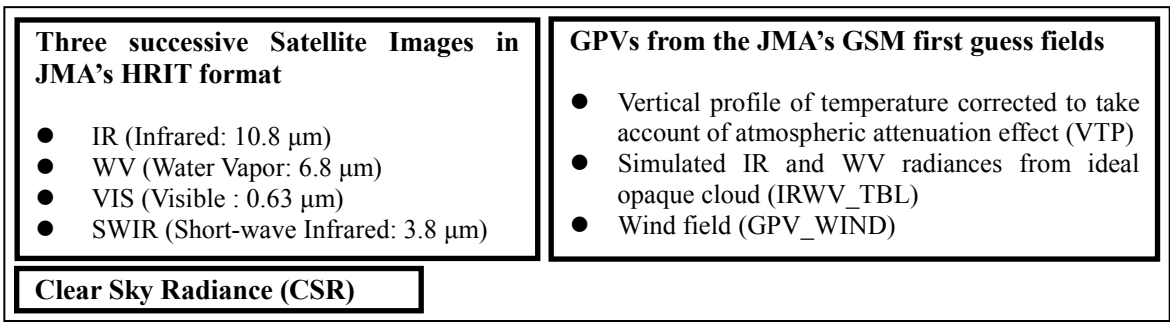

Figure 2: Input data for AMV derivation at JMA/MSC.

2.1 Target selection

The target selection process is performed to select targets to be tracked, e.g. patterns of cirrus clouds for high-level clouds and cumulous clouds for low-level clouds in IR images, or clouds/water vapor patterns in WV images. The target is used to derive a motion vector in the Feature tracking process described in Section 2.2. A small, constant-sized image segment

containing the target (hereafter called a "template image") is used to extract targets from the image. Table 2 shows image pixel size and wavelength for each MTSAT-1R image, and Table 3 shows the template image sizes. The template image size was 32 pixels for derivations of IR, WV, VIS and SWIR AMVs until 04UTC on 19 May 2009. At 05UTC on 19 May 2009, the template image sizes for IR, WV and SWIR AMVs were redefined depending on the image pixel size and image interval. Since the redefinition, 16 and 24 pixels have been applied to the AMV derivations from images at intervals of 15 minutes, and 30 and 60 minutes, respectively. On the other hand, the template image size of 32 pixels is still being applied to VIS AMVs because the pixel size of VIS images is smaller. Specifically, it is a quarter the size of IR, WV and SWIR images.

Table 2: Wavelength and image pixel size of MTSAT-1R image

Channel	VIS	IR	IR2 *	WV	short-wave IR
Wavelength (micrometer)	0.63 (0.55～0.90)	10.8 (10.3～11.3)	12 (11.5～12.5)	6.8 (6.5～7.0)	3.8 (3.5～4.0)
Resolution at Nadir (km)	1	4	4	4	4

* The image of IR2 is not used in the AMV derivation at JMA/MSC.

Table 3: Preset parameters for cross-correlation matching since 05UTC, 19 May 2009

Image interval (minute)	AMV type	Direction	Template image size (unit: pixel)	Search area image size (unit: pixel)	
				For $vector_{coarse}$	For $vector_{fine}$
15	High- and middle-level IR AMVs	Latitudinal	16	32 (=32×1)	32
		Longitudinal	16	96 (=32×3)	32
	WV AMVs	Latitudinal	16	32 (=32×1)	32
		Longitudinal	16	96 (=32×3)	32
	Low-level IR AMVs	Latitudinal	16	32 (=32×1)	32
		Longitudinal	16	64 (=32×2)	32
	SWIR IR AMVs	Latitudinal	16	32 (=32×1)	32
		Longitudinal	16	64 (=32×2)	32
	VIS AMVs	Latitudinal	32	192 (=64×3)	64
		Longitudinal	32	256 (=64×4)	64
30	High- and middle-level IR AMVs	Latitudinal	24	64 (=64×1)	64
		Longitudinal	24	192 (=64×3)	64
	WV AMVs	Latitudinal	24	64 (=64×1)	64
		Longitudinal	24	192 (=64×3)	64
	Low-level IR AMVs	Latitudinal	24	64 (=64×1)	64
		Longitudinal	24	128 (=64×2)	64
	SWIR AMVs	Latitudinal	24	64 (=64×1)	64
		Longitudinal	24	128 (=64×2)	64
	VIS AMVs	Latitudinal	32	192 (=64×3)	64
		Longitudinal	32	256 (=64×4)	64
60	High- and middle-level IR AMVs	Latitudinal	24	128 (=64×2)	64
		Longitudinal	24	320 (=64×5)	64
	WV AMVs	Latitudinal	24	128 (=64×2)	64
		Longitudinal	24	320 (=64×5)	64
	Low-level IR AMVs	Latitudinal	24	128 (=64×2)	64
		Longitudinal	24	192 (=64×3)	64
	SWIR AMVs	Latitudinal	24	128 (=64×2)	64
		Longitudinal	24	192 (=64×3)	64
	VIS AMVs	Latitudinal	32	320 (=64×5)	64
		Longitudinal	32	384 (=64×6)	64

(Notes)
The image intervals for MTSAT-1R are described in Table 1.

Every type of AMV is computed on 0.5 degree latitude/longitude grids within the area of 60S-60N and 90E-170W. Furthermore, the computation area is limited to within a satellite zenith angle of 65 degrees. Before the AMV upgrade on 19 May 2009, the area was 50S-50N and 90E-170W within a satellite zenith angle of 60 degrees. VIS AMVs are computed over regions with solar zenith angles less than 85 degrees (i.e., only daytime regions) while SWIR AMVs are computed over regions with solar zenith angles more than and equal to 85 degrees (i.e., only nighttime regions). In addition to the limitation on area, low-level (below 700 hPa level) IR AMVs, VIS AMVs and SWIR AMVs are not computed over land because the computation accuracy is low.

After these geographical screenings, template images for derivations of respective AMVs are extracted from the second image (B image). For low-level IR, VIS and SWIR AMVs, the center of each template image is placed on the original 0.5 degree latitude/longitude grid point. Meanwhile, the best template image for each AMV position is reselected from twenty-five positions around the original grid using entropy (Imai and Oyama, 2008) for high- (above 400 hPa level) and middle- (400-700 hPa level) level IR and WV AMVs, as shown in Figure 3. In this scheme, entropy is calculated using Equation 1 for every twenty-five template image candidates with positions within the five pixel/line box located at the original grid point.

$$Entropy = -\sum_{DN} P(DN) \times \log_2 P(DN) \quad \text{(Equation 1)}$$

P(DN) is the normalized frequency function of count DN: 0-1023, which is linear with respect to radiance for the image. IR and WV counts are used to generate P(DN) for high- and middle-level IR AMVs and WV AMVs, respectively. For high- and middle-level IR AMVs in particular, the summation in Equation 1 is only found for pixels corresponding to high- and middle-level clouds to avoid including ground pixels and low-level cloud pixels. Finally, one template image candidate with maximum entropy is selected as the final template image. The reselection of a template image is not applied to the target selection without a WV image when reprocessing AMVs from images of GMS-1, -3 and -4.

In the next step, each template image is checked by analyzing the 1-dimensional Equivalent Brightness Temperature of Blackbody (TBB) histogram of a template image (JMA/MSC, 1980). Figure 4 illustrates the schema of the histogram analysis. For IR AMVs, VIS AMVs and SWIR AMVs, the IR template image is checked if it contains enough cloud by analyzing the IR TBB histogram generated from the IR TBBs of the template image. The type of cloud is also inferred in the process. The WV template image is checked in the case of WV AMVs if it contains enough water vapor and cloud by analyzing WV TBB histogram.

Table 4 (a) and (b) list the preset thresholds and the variables used in the diagram of Figure 4. The values are set for (i) Low-level AMVs, (ii) high- and middle-level IR AMVs and (iii) WV AMVs. The goal is to select low-level clouds (e.g. cumulous clouds) for low-level IR AMVs, mainly cirrus clouds for high- and middle-level IR AMVs, and water vapor patterns for WV AMVs.

Each template image is checked in three ways, temperature range of target, thickness of target layer and cloud amount in target.

Condition 1 (Check of the temperature range of the target)

A check of the temperature range of the target is performed to check whether the TBBs of the template image are within the preset temperature range. In this check, TBB_{Min} (TBB_{Max}) is calculated by analyzing the TBB histogram and using TBB at X% (Y%) of total frequency from coldest (warmest) TBB. Here, X and Y are

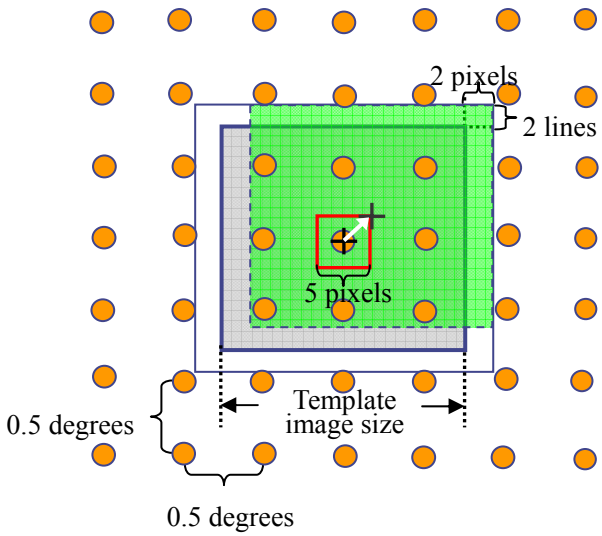

Figure 3: Schematic diagram for reselecting a template image for high- and middle-level IR AMVs and WV AMVs.

Orange circles: 0.5 degree latitude/longitude grid points (original grid points).
Gray square area: Original location of the template image at the original grid point.
Black cross: Position of the template image.
Green square area: Reselected template image with the maximum entropy value of twenty-five candidates.
Red square: The area containing twenty-five pixel positions of template image candidates around the original grid point.

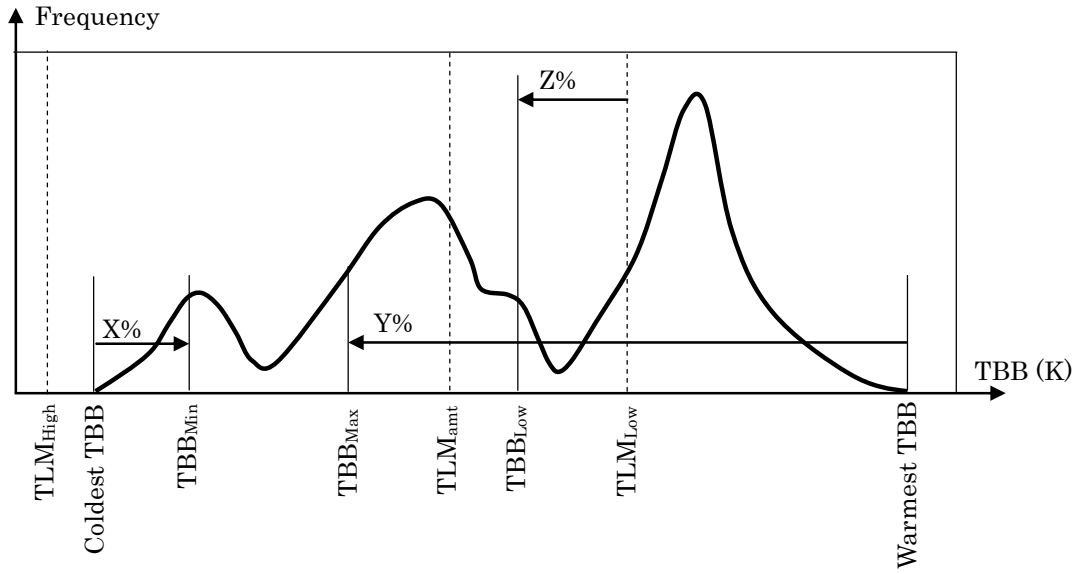

Figure 4: Schematic diagram for the TBB histogram analysis scheme described by JMA/MSC (1980). The bold solid curve represents the TBB histogram frequency generated from pixel-TBBs of a template image. The TBB histogram for IR AMVs, VIS AMVs and SWIR AMVs is generated from the IR TBBs of a template image, while the TBB histogram for WV AMVs is generated from the WV TBBs.

Table 4: Threshold values for the TBB histogram analysis scheme described by JMA/MSC (1980). The TBB histogram for analyzing template images for IR AMVs, VIS AMVs and SWIR AMVs is generated from the IR TBBs of a template image, while that for WV AMVs is generated from the WV TBBs.

(a) THRESHOLD VALUES AND PARAMETERS FOR CALCULATING PARAMETERS IN TABLE 4 (b)

	Descriptions	Low-level IR, VIS and SWIR AMVs	High- and middle-level IR	WV AMVs
PLM_{Low}	Limit of lower pressure level	950 hPa	500 hPa	500 hPa
PLM_{High}	Limit of upper pressure level	650 hPa	150 hPa	150 hPa
PLM_{amt}	Limit of lower pressure level for calculating cloud or water vapor amount	850 hPa	500 hPa	500 hPa
TLM_{Low}	Temperature converted from PLM_{Low} by using vertical temperature profile (VTP) or clear sky radiance data	–	–	–
TLM_{High}	Temperature converted from PLM_{High} by using VTP	–	–	–
TLM_{amt}	Temperature converted from PLM_{amt} by using VTP	–	–	–
X	Percentage of total number of pixels for determining TBB_{Min}	0.1%	0.1%	10.1%
Y	Percentage of total number of pixels for determining TBB_{Max}	99.9%	99.9%	89.9%
Z	Percentage of total number of pixels for determining TBB_{Low}	1.0%	1.0%	1.0%
T_1	Colder limit for thickness of the target cloud or water vapor layer	2.0 ℃	2.0 ℃	2.0 ℃
T_2	Warmer limit for thickness of the target cloud or water vapor layer	35.0 ℃	60.0 ℃	40.0 ℃
C_{min}	Lower limit of amount of target cloud or water vapor layer	1.0%	5.0%	0.5%
C_{max}	Higher limit of amount of target cloud or water vapor layer	100%	99%	100%

(b) PARAMETERS DETERMINED FROM THE FEATURE OF TBB HISTOGRAM

	Description
TBB_{Min}	TBB at X% of total frequencies from the coldest TBB
TBB_{Max}	TBB at Y% of total frequencies from the warmest TBB
TBB_{Low}	TBB at Z% of total frequencies from TLM_{Low} toward coldest TBB
C_{amt}	Cloud or water vapor amount which is percentage of cloud colder than TLM_{amt}

(NOTE) X, Y, Z, TLM_{Low} and TLM_{amt} are explained in Table 4 (a). Coldest and warmest TBBs are shown in Figure 4.

preset parameters. The TBBs should satisfy the following condition:

$$TBB_{Min} < TLM_{Low} \quad \text{and} \quad TBB_{Max} > TLM_{High} \qquad \text{(C-1)}$$

TLM_{Low} and TLM_{High} are the threshold temperatures which are converted from the preset pressure thresholds, PLM_{Low} and PLM_{High}, respectively by referring to VTP.

Condition 2 (Check of the thickness of the target layer)

A check of the thickness of clouds in the target layer (i.e., the clouds and/or water vapor layer) is performed to eliminate multi-layered clouds. In this check, TBB_{Low} and TBB_{Min} are used to analyze the TBB histogram. TBB_{Low} is defined as TBB at preset constant Z% of total frequencies from TLM_{Low} toward the coldest TBB, while TBB_{Min} is defined as TBB at X% of total frequencies from the coldest TBB. Here, TLM_{Low} is the temperature that is converted from the preset constant pressure level, PLM_{Low}, by referring to VTP or CSR data.

The TBB histogram should satisfy this condition:

$$T1 < TBB_{Low} - TBB_{Min} < T2 \qquad \text{(C-2)}$$

T1 and T2 are the preset colder and warmer temperature limits for thickness of target area as described in Table 4 (a).

Condition 3 (Check of cloud amount in target)

A check on the cloud amount in the target is performed

to check whether the template image contains adequate clouds and/or water vapor patterns. In this check, cloud amount which is the percentage of cloud colder than TLM_{amt}, C_{amt}, is used to analyze the TBB histogram. Here, TLM_{amt} is the temperature that is converted from the preset constant pressure level, PLM_{amt}, by referring to VTP. Finally, the TBB histogram should satisfy the following condition:

$$Cmin <= Camt <= Cmax \qquad (C\text{-}3)$$

C_{min} and C_{max} are the preset percentages, i.e., the lower and higher limits of cloud amounts in the target layer.

Finally, template images for respective AMVs are selected using these three conditions. For high- and middle-level IR AMVs, the template image is selected so that the cloud pixels with heights between 150 hPa (PLM_{High}) and 500 hPa (PLM_{Low}) occupy 5 (C_{min}) to 99% (C_{max}) of the whole template image. For low-level AMVs, the template image is selected so that the cloud pixels with heights between 650 hPa and 950 hPa occupy 1 to 100% of the whole template image. For WV AMVs, the template image is selected so that the water vapor layer and/or cloud layer between 150 hPa and 500 hPa occupy 0.5 to 100% of the whole template image.

In the final step, every template image is checked for whether it contains cumulonimbus clouds or not, based on the difference between IR and WV TBBs within the template image. If a template image contains cumulonimbus clouds, it is rejected.

2.2 Feature tracking

Following Target selection, a displacement vector for each template image is derived by tracking clouds and/or water vapor patterns within the template image using the successive images. JMA/MSC uses a cross-correlation matching scheme to derive displacement vectors, which is the most general methodology and is also used by most of the foreign satellite centers, such as NOAA/Satellite and Information Service (NESDIS) and the European Organization for the Exploitation of Meteorological Satellites (EUMETSAT). Figure 5 illustrates the procedure of cross-correlation matching described by JMA/MSC (1980). One cross-correlation coefficient matrix CC(p, q) is obtained when correlation values between template images and search area images are calculated in counts (0-1023) linear with respect to radiance for respective points within the lag area. The definition of CC(p, q) is given by Equation 2. The position (p, q) with the largest correlation coefficient value within the lag area is adopted as the best matched position.

$$CC(p,q) = \frac{\sum_{i=1,j=1}^{M} (T(i,j) - < T >)(S(i+p, j+q) - < S(p,q) >)}{\sqrt{\sum_{i=1,j=1}^{M} (T(i,j) - < T >)^2} \sqrt{\sum_{i=1,j=1}^{M} (S(i+p, j+q) - < S(p,q) >)^2}} \qquad \text{(Equation 2)}$$

M : Template image size,　N : Search area image size (M < N)
T (i, j) : Counts (0-1023) for pixels within the template image
<T> : Average of T
S (i+p, j+q) : Counts (0-1023) for pixels within the search area image
<S(p, q)> : Average of S
i, j : Location in pixel-line coordinates in the template image (i, j= 1, .. , M)
p, q : Lag position on cross-correlation coefficient matrix (p, q =－(N－M) /2, … , (N－M) /2)

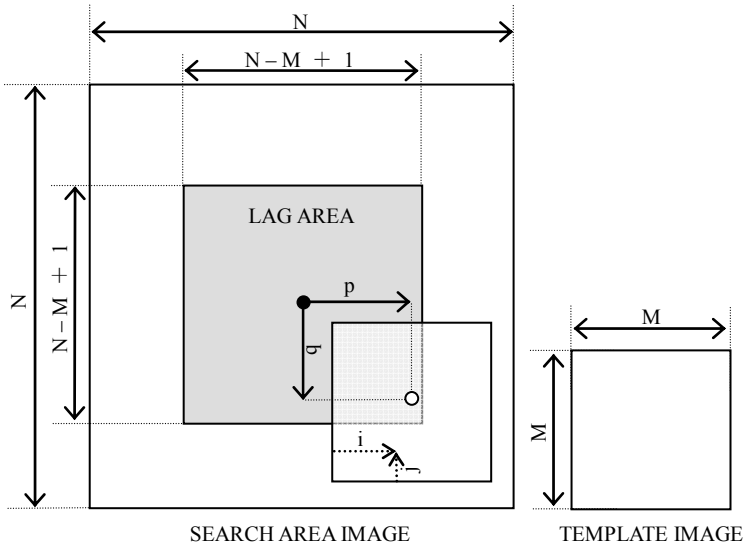

Figure 5: Illustration of a template image, search area image and Lag area (JMA/MSC, 1980)

Table 5: Filtering conditions for internal Quality Control in feature tracking and height assignment.

FILTERING CONDITIONS FOR INTERNAL QUALITY CONTROL

(a) FEATURE TRACKING

Check item	AMV type	Conditions to reject vectors
Speed Consistency	High- and middle-level IR AMVs WV AMVs	$10.0m/s \le \lvert WindSpeed(AB) - WindSpeed(BC) \rvert$
	Low-level IR AMVs VIS AMVs SWIR AMVs	$5.0m/s \le \lvert WindSpeed(AB) - WindSpeed(BC) \rvert$
Lower limit of speed	High- and middle-level IR AMVs WV AMVs	$WindSpeed(AB) < 2.5m/s \quad or \quad WindSpeed(BC) < 2.5m/s$
	Low-level IR AMVs VIS AMVs SWIR AMVs	$WindSpeed(AB) < 1.0m/s \quad or \quad WindSpeed(BC) < 1.0m/s$

(b) HEIGHT ASSIGNMENT

Check item	AMV type	Conditions to reject vectors
Height Consistency	All types	$130\,hPa \le \lvert Height(A) - Height(B) \rvert$ *or* $130\,hPa \le \lvert Height(B) - Height(C) \rvert$ *or* $130\,hPa \le \lvert Height(C) - Height(A) \rvert$

(NOTE)
A, B, and C in the tables represent the first image, the second image and the third image, respectively, of the three successive images which are used in the AMV computation.
AB and BC represent two wind vectors derived from A and B, and B and C images, respectively.

Table 3 lists the sizes of template images and search area images in current use. JMA/MSC uses the three successive images, A (first), B (second) and C (third), in Feature tracking. With the B template image, cross-correlation matching is performed using images A and B, and images B and C to derive the two wind vectors, AB and BC. Matching for each wind vector is performed in two steps, i.e., coarse matching and fine matching.

Coarse matching is performed to derive the large scale wind field, where $vector_{coarse}$ is derived from the coarse images, e.g., 64×n pixel by 64×m line images (n and m are integer values) which are each spatially sampled by rates n and m respectively.

Following coarse matching, fine matching is done to

derive the fine displacement vector. $Vector_{fine}$ is derived from the images with the original resolution for fine tuning the displacement. $Vector_{fine}$ is derived in two steps. First, the base $vector_{fine}$ is computed as a displacement vector in pixel units (Hereafter, the position with the largest correlation coefficient within matrix CC(p, q) is referred to as (p_{max}, q_{max})). Second, the sub-pixel displacement vector is computed by estimating the correlation peak position of the approximated ellipsoidal curved surface of CC(p, q). Finally, the final $vector_{fine}$ is given as the vector sum of the base $vector_{fine}$ and the sub-pixel displacement vector.

The vector sum of $vector_{coarse}$ and the final $vector_{fine}$ is the resultant vector. However, the resultant vectors with poor quality are rejected by internal quality control based on the conditions in Table 5 (a). The final output vector is the second vector derived from images B and C (vector BC).

2.3 Height assignment

Height assignment is one of the most important processes for determining AMV quality as well as Feature tracking. JMA/MSC chooses an appropriate height assignment scheme for each type of AMV. The height level of AMV is computed for the three successive images, A (first), B (second) and C (third). For internal quality control, AMVs with poor quality are rejected based on the conditions in Table 5 (b). The height level derived from image C is used as the final output.

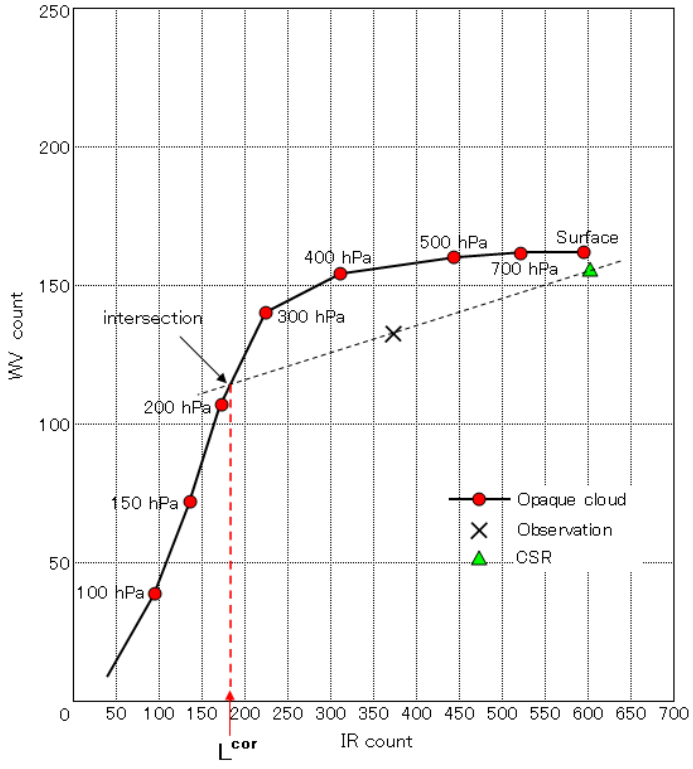

Figure 6: Illustration of the H2O-IRW intercept method which corrects the radiance for semi-transparent clouds. The vertical and horizontal axes are WV and IR counts, respectively. The solid curve represents model calculations for opaque clouds. Red circles along the curve correspond to Surface, 700-, 500-, 400-, 300-, 200-, 150-, and 100-hPa altitudes. The black broken line is drawn from the Clear Sky Radiance (CSR) (Triangle) through the observed radiances of one pixel (Cross) within the template image. The intersection of this line with the solid curve provides the estimation of cloud radiance.

(a) Height for high- and middle-level IR AMVs

In general, the height of cirrus cloud which is known as a good tracer is replaced by the height of the uppermost (coldest) cloud within the template image. However, in many cases, radiances from most of the cirrus clouds are contaminated by the surface radiance due to their semi-transparency to radiation (i.e., cirrus clouds are not always treated as black bodies). Therefore, JMA/MSC uses the H2O-IRW intercept method (Nieman et al., 1993; Schmetz et al., 1993) to estimate correct IR and WV radiances corresponding to high-level semi-transparent clouds without radiance contamination.

Figure 6 illustrates application of the H2O-IRW intercept method. The correct IR and WV radiances from clouds are estimated by referring to CSR and the IR and WV radiance profiles from ideal opaque clouds (IRWV_TBL). IRWV_TBL is simulated using a Radiative Transfer Model (RTM) and forecast profiles of temperature and humidity. In advance, to mitigate the forecast error and interpolation error on time and space, IRWV_TBL is corrected by using the observed IR and WV radiances within the template image (JMA, 2007; Imai and Oyama, 2008). Hereafter, the corrected IR radiance is referred to as L^{cor}, which is drawn in Figure 6 as well.

After using the H2O-IRW intercept method to correct the radiance for each cloud pixel within the template image, cloud pixels contributing to the AMV height are selected from the template image. Since 05UTC on 19 May 2009, the new height assignment scheme suggested by Oyama et al. (2008) has been used to derive the height levels of high- and middle-level IR AMVs instead of the most frequent cloud height level (P_{FREQ}) which is mentioned in Section 2.3 (b) regarding the height assignment of WV AMVs. The new height assignment scheme was introduced to improve some erroneous height assignments in the previous IR AMVs, which were caused by not considering the contribution rate of each cloud pixel to feature tracking. The erroneous height assignment led to fast speed bias at middle level and a smaller number of AMVs at high level for the previous IR AMVs. In the new scheme, each pixel (i, j) contribution rate to feature tracking (hereafter referred to as CCij) is introduced. CCij can be computed in the feature tracking process under cross-correlation matching described in Section 2.2. The formulation of CCij is described by Equation 3a and 3b (Büche et al., 2006).

CC_{max} is the cross-correlation value at the location (p_{max}, q_{max}) in Section 2.2, which is the maximum of the cross-correlation matrix CC(p, q) in fine matching.

To derive the height level of each AMV, the representative IR radiance from clouds (hereafter referred to as L1) is computed by weighting pixel IR radiances by their individual CCij values. The definition of L1 is Equation 4.

$$CC_{\max} = \frac{\sum_{i=1,j=1}^{M} (T(i,j) - < T >)(S(i+p_{\max}, j+q_{\max}) - < S(p_{\max}, q_{\max}) >)}{\sqrt{\sum_{i=1,j=1}^{M} (T(i,j) - < T >)^2} \sqrt{\sum_{i=1,j=1}^{M} (S(i+p_{\max}, j+q_{\max}) - < S(p_{\max}, q_{\max}) >)^2}} = \sum_{i=1,j=1}^{M} cc_{ij} \qquad \text{(Equation 3a)}$$

$$CC_{ij} = \frac{(T(i,j) - < T >)(S(i+p_{\max}, j+q_{\max}) - < S(p_{\max}, q_{\max}) >)}{\sqrt{\sum_{i=1,j=1}^{M} (T(i,j) - < T >)^2} \sqrt{\sum_{i=1,j=1}^{M} (S(i+p_{\max}, j+q_{\max}) - < S(p_{\max}, q_{\max}) >)^2}} \qquad \text{(Equation 3b)}$$

$$L1 \equiv \frac{1}{\sum_{0<CCij\,(except\ for\ background)} CC_{ij}} \sum_{0<CCij\,(except\ for\ background)} L_{ij}^{cor} \times CC_{ij} \qquad \text{(Equation 4)}$$

L^{cor}_{ij} is the IR radiance for each pixel (i, j) corrected by the H2O-IRW intercept method. L1 is computed by using only cloudy-pixel IR radiances with CCij values greater than 0.

Before computing L1, background pixels within the template image should be defined. The schematic diagram for a feature tracking for cirrus cloud is shown in Figure 7. Figure 7 (a) represents the distributions of IR radiances for the template image and Figure 7 (b) represents the searched image segment within the search area image. Figure 7 (c) shows the CCij values for the template image, which are computed from the IR radiance data of Figure 7 (a) and (b). The larger CCij values in Figure 7 (c) correspond to cirrus clouds with smaller IR radiances in Figure 7 (a) and (b).

Figure 7 (d) shows the scatter plots of CCij values against the original IR radiance for the template image. L1 is computed by using only cloudy pixels with CCij values greater than 0, i.e., pixels with CCij values less than 0 (in the yellow area in Figure 7 (d)) and values corresponding to the background (in the grey area in Figure 7 (d)) are excluded from the L1 computation.

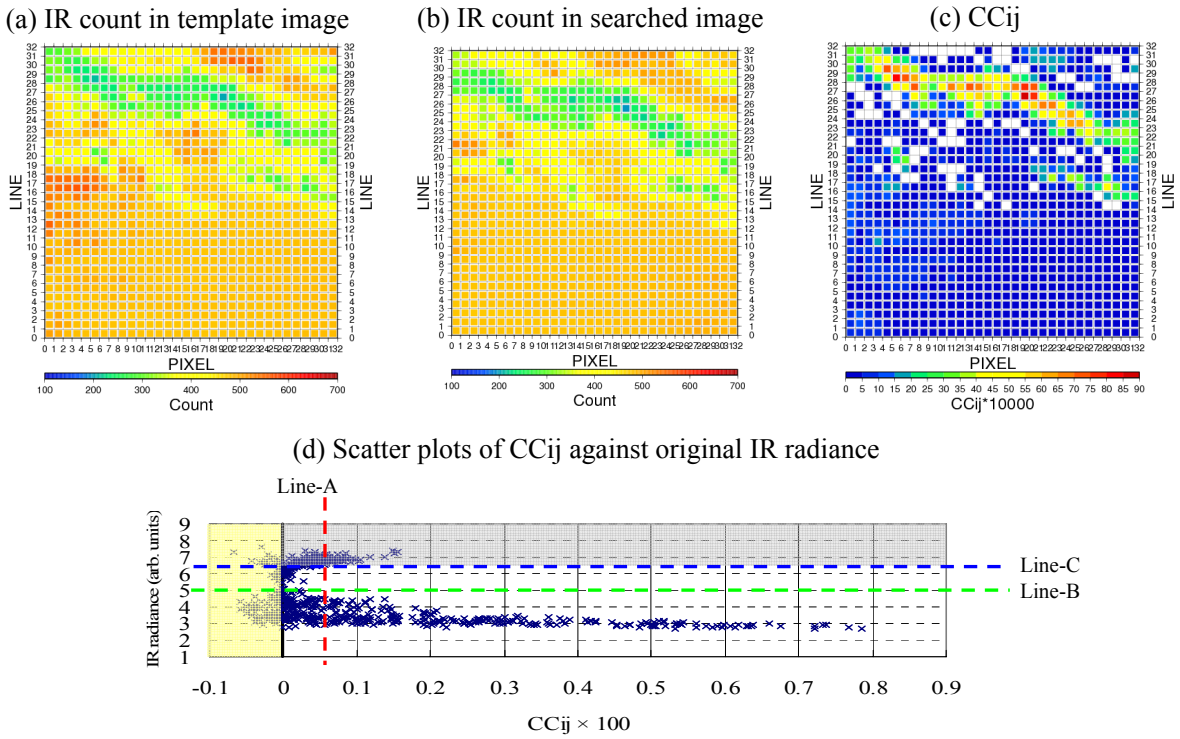

Figure 7: Schematic diagram for the pixel selection in the height assignment of high- and middle- level IR AMVs (Oyama et al., 2008). An example is shown for a template image (size = 32 pixels) at (35S, 131E) at 12UTC on 10 March 2007.

(a) The distribution of original IR count (0-1023) linear with respect to radiance for the template image.
(b) The distribution of original IR count for the searched image segment in the search area.
(c) CCij derived from original IR counts of Figure 7 (a) and (b).
(d) Scatter plots of CCij against original IR radiance in the template image.
Red line (Line-A): Average of CCij within the template image
(= cross-correlation coefficient between (a) and (b) images / (template image size)^2).
Green line (Line-B): Line defined as IR radiance = the average of original IR radiance.
Blue line (Line-C): Line defined as IR radiance = the IR radiance at the intersection of Line-A with the quadratic curve of pixel-distribution.

Pixels within the grey area in Figure 7 (d) are defined as background pixels for Equation 4.

L1 is finally converted to the representative temperature (T_{REP}) using MTSAT-1R's conversion table between IR channel radiance and temperature. Then, T_{REP} is converted to the AMV height level by referring to VTP. However, in order to compensate for the insufficiency of the target selection, the AMV assigned to a height level lower than 400 hPa by using L1 are additionnally examined on the cloud type by checking correlation values between the IR and WV template images (Xu et al., 1998). If the correlation value is smaller than 0.35, the target cloud for the AMV is treated as low level, and reassigned to a height level computed using the original IR TBBs of the cloud and referring to VTP.

Equation 4 is modified without the WV image. The modified equation is applied to the AMV reprocess from GMS-1, 3 and 4 without the WV channel sensor in the AMV reprocess for JRA-55 and SCOPE-CM. L^{cor}_{ij} in Equation 4 is replaced with the original IR radiance of each pixel (i, j). Furthermore, L1 is computed as the weighted mean of the original IR radiances smaller than the original IR radiance average (Line-B in Figure 7 (d)) for cloud pixels with CCij greater than 0. L1 is converted to T_{REP} using the conversion table between IR radiance and temperature, then T_{REP} is converted to AMV height level by referring to VTP.

(b) Height for WV AMVs

The height level of cloudy-region WV AMVs have been computed as the most frequent cloud height level within the template image, P_{FREQ}, since 06UTC on 30 May 2007 (JMA, 2007; Imai and Oyama, 2008). P_{FREQ} is computed as shown in Figure 8. First, the height-level histogram is generated from the cloud-pixel height levels within the template image. The cloud-pixel height levels are those that have been converted from L^{cor} using MTSAT-1R's conversion table between IR channel radiance and temperature, and referring to VTP. Second, the 50-hPa height histogram is introduced, which is the accumulated height-level histogram in 50 hPa intervals. The aims of introducing the 50-hPa height histogram are: (1) to take the thickness of cirrus clouds into account, and (2) to avoid selecting some accidental frequent height-levels, which are mainly caused by small sampling errors in selecting peaks from the original height-level histogram with a resolution of 1 hPa or less. The most frequent height-level rank ($P50_{FREQ}$) is extracted from the 50-hPa height histogram. P_{FREQ} is the most frequent height level of the height levels within the rank of $P50_{FREQ}$.

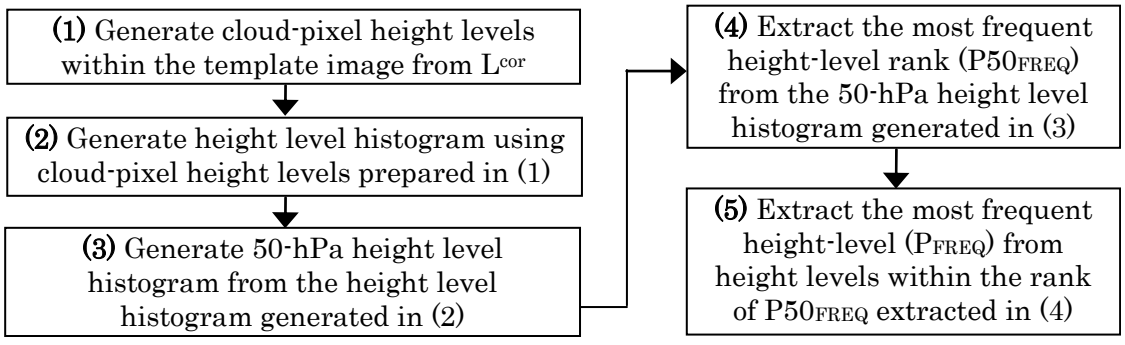

Figure 8: Flow chart for computing the most frequent cloud height level (P_{FREQ}).

After these steps, the AMV is categorized into cloudy-region and clear-sky region WV AMVs. If the P_{FREQ} of the AMV is higher than 400 hPa, the AMV is treated as having been derived by tracking high-level clouds and/or water vapor patterns, and is categorized as a cloudy-region WV AMV. The height level is set to P_{FREQ}. Otherwise, if the P_{FREQ} is lower than 400 hPa, the AMV is categorized as a clear-sky region WV AMV and the height level is set to a height level computed by using the average of WV TBBs (Ohkawara et al., 2004).

(c) Height for Low-level IR AMVs

A low-level IR AMV is assigned to the cloud base height of low-level clouds, e.g. cumulous clouds, using the scheme formulated by Tokuno (1998). As seen in Figure 9, the cloud base temperature, $T_{(base)}$, is estimated by using the mean and standard deviation of IR TBBs corresponding to the cloud top, then the cloud base height is computed from $T_{(base)}$ referring to VTP. If the cloud base height is higher than the 850 hPa level, the AMV is reallocated to the fixed 850 hPa level.

(d) Height for VIS AMVs and SWIR AMVs

VIS AMVs and SWIR AMVs are assigned to the cloud base height of low-level clouds based on the Tokuno scheme (1998) as low-level IR AMVs.

2.4 Computations of the QI and the RFF quality flag

After completing Height assignment, the QI and the RFF quality flag are attached to respective AMVs. The QI and the RFF quality flag are computed with reference to JMA's NWP (GSM) first-guess field under EUMETSAT (Holmlund, 1998) and the Cooperative Institute for Meteorological Satellite Studies of the University of Wisconsin-Madison (UW-CIMSS) (Olander, 2001) guidelines, respectively.

QI is presently used as the main AMV quality metric by most operational NWP centers for data assimilation in their NWP models. QI for each AMV is derived based on the properties of the vector itself and its consistency with neighboring vectors. Five tests are performed: (i) Direction consistency, (ii) Speed consistency and (iii) Vector consistency using the two intermediate vectors from three successive images (vectors AB and BC) in feature tracking, (iv) Forecast consistency using JMA's GSM first-guess wind field (GPV_WIND), and (v) Spatial consistency using adjacent AMV data. Lastly, QI with/without a forecast consistency check are calculated as a linear weighted mean of the quality components obtained from the five tests.

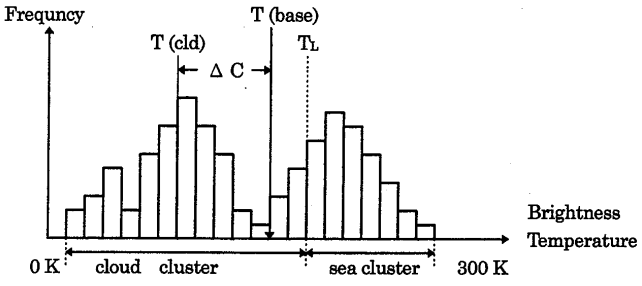

Figure 9: Schematic diagram for computing cloud base height at JMA/MSC (Tokuno, 1998).
T_L : Boundary brightness temperature between cloud and sea clusters.
$T_{(cld)}$: Mean temperature of the cloud cluster.
$T_{(base)}$: Cloud base temperature.
⊿C : $\sqrt{2} \times \sigma$ (σ is the TBB standard deviation of the cloud cluster).

In the process of computing the RFF quality flag, the height level of the AMV is adjusted to minimize a variational penalty function, which is evaluated using the AMV data and NWP first-guess fields. The RFF quality flag is computed from the resultant outputs.

The QI and RFF quality flag range from 0 to 1. The large value indicates high quality in both of the indexes.

2.5 Data disseminations and quality monitoring

The final output of the AMV data is stored with QI with/without a forecast consistency check and RFF quality flag in BUFR and JMA's internal data format (DCDH). BUFR is disseminated to users via GTS and used in the JMA's NWP, whereas DCDH is only used in the JMA's NWP.

JMA/MSC monitors the monthly quality of AMVs against sonde observations, and the wind profiler observations from the JMA observation stations. In both of the statistics, AMVs with QI (with forecast consistency check) above 0.85 are used.

3. Improvements of AMV quality by upgrades on 19 May 2009

This section describes the quality improvements of MTSAT-1R AMVs brought about by the upgrades of the AMV derivation at 05UTC on 19 May 2009. The outline of the upgrades is shown below:

(1) Upgrade of height assignment scheme for high- and middle-level IR AMVs

Previously, the high- and middle-level (above 700 hPa) IR AMVs were assigned to the most frequent cloud height level (P_{FREQ}, mentioned in Section 2.3 (b)). In the previous IR AMVs, there were problems due to some erroneous height assignments, namely, less AMV data than the ordinary above 400 hPa, and a large fast wind speed bias at levels between 500 and 700 hPa. To mitigate these problems, JMA/MSC started using the height assignment scheme directly linked to feature tracking in computing the AMV height level, where each pixel contribution rate to feature tracking (CCij) is introduced.

(2) Resizing template images for IR AMVs and WV AMVs

Using a smaller template image size enables respective air-parcel movement on streamlines to be properly captured, even in flows with large curvatures. Moreover, the smaller template image leads to higher accuracy for height assignment because the probability that a single-layer cloud will dominate the template image increases. To improve the qualities of IR AMVs and cloudy-region WV AMVs, template images for IR AMVs (including SWIR AMVs) and WV AMVs were resized from 32 pixels to 16 or 24 pixels as shown in Table 3. The new template image sizes were determined by investigating the number of high-quality AMVs, as well as the AMV qualities against sonde observation and NWP fields. By making template images smaller, the slow wind speed bias remaining in the previous AMVs, particularly for winter hemispheres, is reduced or mitigated.

(3) Expansion of AMV derivation area

The area for deriving AMVs was expanded from 90E-170W and 50S-50N to 90E-170W and 60S-60N. In addition, the screening condition on satellite zenith angle was changed from 60 degrees to 65 degrees. This area-expansion leads to the possibility of providing AMV data for higher latitudes to users.

In the next section, quality comparisons between the previous and current AMVs for 00 and 12 UTC, which are computed using images taken at an interval of 15 minutes, are shown by using monthly statistics against sonde observations and JMA's GSM first-guess fields. In these statistics, QI with the forecast consistency check

is used as the criterion for data filtering. Hereafter, AMVs computed by the previous (before the upgrade) and current derivation algorithms are referred to as previous AMVs and current AMVs, respectively.

3.1 Results on monthly statistics of AMV quality to sonde observations

Table 9 and 10 show the monthly statistics (Root Mean Square Vector Difference (RMSVD), wind speed bias (BIAS) and number) against sonde observations for the previous and current AMVs for January and July 2009. The statistics were taken for the Northern Hemisphere (20N-60N), Southern Hemisphere (SH: 60S-20S) and Tropics (TR: 20S-20N). AMVs with QI above 0.85 are used in the statistics.

With respect to the statistics for January 2009 in Table 9, the most distinct improvement of the current AMVs from the previous AMVs is the mitigation of slow BIAS found in high-level IR AMVs in the winter hemisphere. The slow BIAS of the current AMVs is smaller than that of the previous AMVs for NH. Meanwhile, for TR and SH, the BIASes of the previous AMVs are slightly negative while those of the current AMVs are slightly positive. The differences between the previous and current AMVs are recognized in accordance with the wind speed increases of the current AMVs from the previous AMVs. The RMSVDs of the current AMVs are slightly smaller than those of the previous AMVs for NH and SH. The number of the current AMVs is larger than that of the previous AMVs for SH while the opposite situation is true for TR. Similar situations have been discovered in the statistics for middle-level IR AMVs as in high-level IR AMVs. For low-level IR AMVs, the difference of RMSVD between the previous and current AMVs is very small for NH, SH and TR. The BIAS of the current AMVs is slightly smaller than that of the previous AMVs for NH and SH, however, it is slightly larger for TR. As for number, the number of the current AMVs is larger for NH and SH, but smaller for TR than that of the previous AMVs. In particular, the rate of increase of the current AMVs from the previous AMVs for SH is large at about 42%. For cloudy-region WV AMVs, the difference of RMSVD between the current AMVs and previous AMVs is small for NH, SH and TR. Meanwhile, the BIAS of the current AMVs is slightly more positive than that of the previous AMVs for NH, SH and TR. For SWIR AMVs, similar situations have been discovered in the statistics on BIAS and RMSVD as in low-level IR AMVs.

With respect to the statistics for July 2009 shown in Table 10, the most distinct improvement in the current AMVs is the mitigation of slow BIAS for high-level IR AMVs, just as in January 2009. For high-level IR AMVs, the slow BIASes of the current AMVs are smaller than that of the previous AMVs for NH and SH. The RMSVDs of the current AMVs are smaller those of the previous AMVs for NH and SH. As for middle-level IR AMVs, the RMSVD of the current AMVs is slightly larger than that of the previous AMVs for NH and SH, yet it is nearly the same as those of the previous AMVs for TR. The BIASes of the current and previous AMVs for NH, TR and SH are nearly the same. As for low-level IR AMVs, the RMSVD and BIAS of the current AMVs are nearly the same as those of the previous AMVs. Just as is the case with the statistics for January 2009, the rate of increase of the number of current AMVs from the previous AMVs is larger for SH compared to the other regions. These situations are similar to those in the statistics for SWIR AMVs. As for cloudy-region WV AMVs, the fast BIASes of the current AMVs are slightly larger than those of the previous AMVs for NH, TR and SH in accordance with the increase of wind speed. These situations are similar to those seen in the statistics for January 2009.

Table 9: Monthly quality of the previous and current AMVs (QI > 0.85) against sonde observations. The statistics are taken for AMVs computed for January 2009.

High-level IR AMVs (above 400 hPa)	NH (20N-60N)		TR (20S-20N)		SH (20S-60S)	
	Previous	Current	Previous	Current	Previous	Current
RMSVD (m/s)	8.37	8.20	5.59	5.61	6.43	6.38
BIAS (m/s)	-2.10	-1.40	-0.12	0.41	-0.20	0.71
WIND SPEED (m/s)	35.06	37.04	13.45	13.92	23.36	25.07
Collocation NUMBER	2770	2363	4572	3591	1967	1557
NUMBER	23819	21278	52369	41706	34959	42827

Middle-level IR AMVs (400 - 700 hPa)	NH (20N-60N)		TR (20S-20N)		SH (20S-60S)	
	Previous	Current	Previous	Current	Previous	Current
RMSVD (m/s)	7.48	7.37	4.49	4.70	6.42	6.21
BIAS (m/s)	-1.62	-0.35	-0.96	-0.84	-0.68	1.05
WIND SPEED (m/s)	27.02	28.25	9.56	11.07	18.27	20.49
Collocation NUMBER	1811	1810	137	56	183	188
NUMBER	14352	16263	1771	1041	7618	15950

Low-level IR AMVs (below 700 hPa)	NH (20N-60N)		TR (20S-20N)		SH (20S-60S)	
	Previous	Current	Previous	Current	Previous	Current
RMSVD (m/s)	4.48	4.52	3.41	3.61	4.31	4.35
BIAS (m/s)	-0.60	-0.35	0.54	0.73	1.09	1.06
WIND SPEED (m/s)	10.95	11.26	10.57	10.63	10.12	10.95
Collocation NUMBER	755	737	755	615	171	126
NUMBER	22816	28800	36622	26593	16694	23775

Cloudy-region WV AMVs	NH (20N-60N)		TR (20S-20N)		SH (20S-60S)	
	Previous	Current	Previous	Current	Previous	Current
RMSVD (m/s)	8.54	8.47	6.02	6.16	6.57	6.89
BIAS (m/s)	0.08	1.05	1.24	1.65	1.64	1.97
WIND SPEED (m/s)	37.52	38.88	15.21	15.68	25.88	27.10
Collocation NUMBER	5387	4201	7593	6296	2827	2747
NUMBER	36635	33891	78139	67621	46500	58930

SWIR AMVs (below 700 hPa)	NH (20N-60N)		TR (20S-20N)		SH (20S-60S)	
	Previous	Current	Previous	Current	Previous	Current
RMSVD (m/s)	4.39	4.39	3.42	3.55	4.34	4.45
BIAS (m/s)	-0.63	-0.30	0.17	0.28	-0.19	0.30
WIND SPEED (m/s)	11.44	11.65	10.21	10.53	11.16	10.90
Collocation NUMBER	330	328	402	334	50	56
NUMBER	10410	13364	19423	15259	6900	8913

To show the impact of making template images smaller on AMV quality excluding the differences of the height assignment scheme and derivation area, Figure 10 shows the monthly statistics against sonde observations for AMVs by using two template image sizes, specifically, 16 pixels (currently used for 6-hourly AMVs) and 32 pixels (previously used size). Both of the AMVs are computed using the common height assignment scheme (current scheme), derivation area (20N-50N and 90E-170W within a satellite zenith angle of less than 60 degrees) and images taken at an interval of 15 minutes as the operational 6-hourly AMVs. Hereafter, these AMVs are referred to by their template image sizes of 16 and 32 pixels as T16 and T32, respectively.

Table 10: Monthly quality of the previous and current AMVs (QI > 0.85) against sonde observations. The statistics are taken for AMVs computed for July 2009.

High-level IR AMVs (above 400 hPa)	NH (20N-60N)		TR (20S-20N)		SH (20S-60S)	
	Previous	Current	Previous	Current	Previous	Current
RMSVD (m/s)	7.02	6.94	5.89	6.13	7.83	7.62
BIAS (m/s)	-0.85	0.28	-0.40	0.30	-1.08	-0.17
WIND SPEED (m/s)	22.78	23.91	15.80	16.41	32.40	32.53
Collocation NUMBER	10938	8760	4999	3905	1210	1002
NUMBER	43258	47408	53028	43017	25095	32077

Middle-level IR AMVs (400 - 700 hPa)	NH (20N-60N)		TR (20S-20N)		SH (20S-60S)	
	Previous	Current	Previous	Current	Previous	Current
RMSVD (m/s)	6.42	6.64	3.91	3.98	7.47	8.13
BIAS (m/s)	0.63	0.28	-0.05	0.07	-1.70	-1.73
WIND SPEED (m/s)	17.15	17.20	9.86	10.52	25.34	26.01
Collocation NUMBER	630	440	294	119	786	931
NUMBER	4129	5268	3272	1868	15966	22854

Low-level IR AMVs (below 700 hPa)	NH (20N-60N)		TR (20S-20N)		SH (20S-60S)	
	Previous	Current	Previous	Current	Previous	Current
RMSVD (m/s)	3.25	3.79	4.17	4.17	4.02	4.19
BIAS (m/s)	-0.13	0.12	0.19	0.24	-0.16	-0.15
WIND SPEED (m/s)	8.72	9.20	9.04	9.27	12.17	12.93
Collocation NUMBER	372	226	502	385	493	425
NUMBER	9177	8013	20863	17268	36731	47096

Cloudy-region WV AMVs	NH (20N-60N)		TR (20S-20N)		SH (20S-60S)	
	Previous	Current	Previous	Current	Previous	Current
RMSVD (m/s)	7.08	7.37	6.61	6.85	8.40	8.13
BIAS (m/s)	0.83	1.54	1.38	1.77	0.21	1.06
WIND SPEED (m/s)	24.35	25.48	17.95	18.41	35.51	35.46
Collocation NUMBER	22954	21637	9074	7626	1541	1404
NUMBER	72798	81592	81134	71866	31412	44589

SWIR AMVs (below 700 hPa)	NH (20N-60N)		TR (20S-20N)		SH (20S-60S)	
	Previous	Current	Previous	Current	Previous	Current
RMSVD (m/s)	3.09	3.21	4.66	4.08	4.04	4.57
BIAS (m/s)	-0.40	-0.15	0.05	1.28	0.09	0.54
WIND SPEED (m/s)	8.32	8.77	8.55	8.89	12.44	12.20
Collocation NUMBER	217	144	208	158	130	100
NUMBER	6063	5443	11810	10700	18283	24283

With respect to high-level IR AMVs, the magnitudes of slow BIAS and RMSVD of T16 are smaller than those of T32 in summer and winter hemispheres, while the number of T16 is less than that of T32. With respect to the cloudy-region WV AMVs, RMSVDs are nearly the same between T16 and T32 in summer and winter hemispheres. On the other hand, BIAS of T16 is slightly positive while that of T32 is slightly negative or nearly zero. The decrease in the number of T16 from T32 is smaller than that for high-level IR AMV.

In the research for the operational MTSAT-1R AMVs computed using images taken at intervals of 30 or 60 minutes, the same positive impact of making template image sizes smaller on BIAS and RMSVD, i.e.,

decreasing BIASes and RMSVDs, was identified (not shown here). However, the decrease of the number was larger than that of the AMVs computed using images taken at interval of 15 minutes. This difference using the images with different intervals is due to the lifetime and deformation of clouds, i.e., using longer time-interval images leads to difficulties in feature tracking. After several impact tests on JMA's NWP side, a larger template image, 24 pixels, was adopted for AMVs computed using images taken at an interval of 30 or 60 minutes.

The impact of making template images smaller on AMV quality was also investigated by Sohn and Borde (2008). They indicated some positive effects, i.e., a mitigation of slow wind speed bias at high level and reduction of height assignment error.

3.2 Results on monthly statistics of AMV quality to JMA's GSM first-guess fields

3.2.1 Height dependency

In this section, the qualities of the previous and current AMVs are investigated in terms of height dependency on JMA's GSM first-guess fields.

Figure 11-1 and 11-2 show the height dependencies of the wind speed bias (BIAS) against JMA's GSM first-guess fields and number (QI > 0.85) for the previous and current IR AMVs. The statistics for the Northern Hemisphere (NH: 20N-60N) and Southern Hemisphere (SH: 60S-20S) and Tropics (TR: 20S-20N) are taken for January and July 2009.

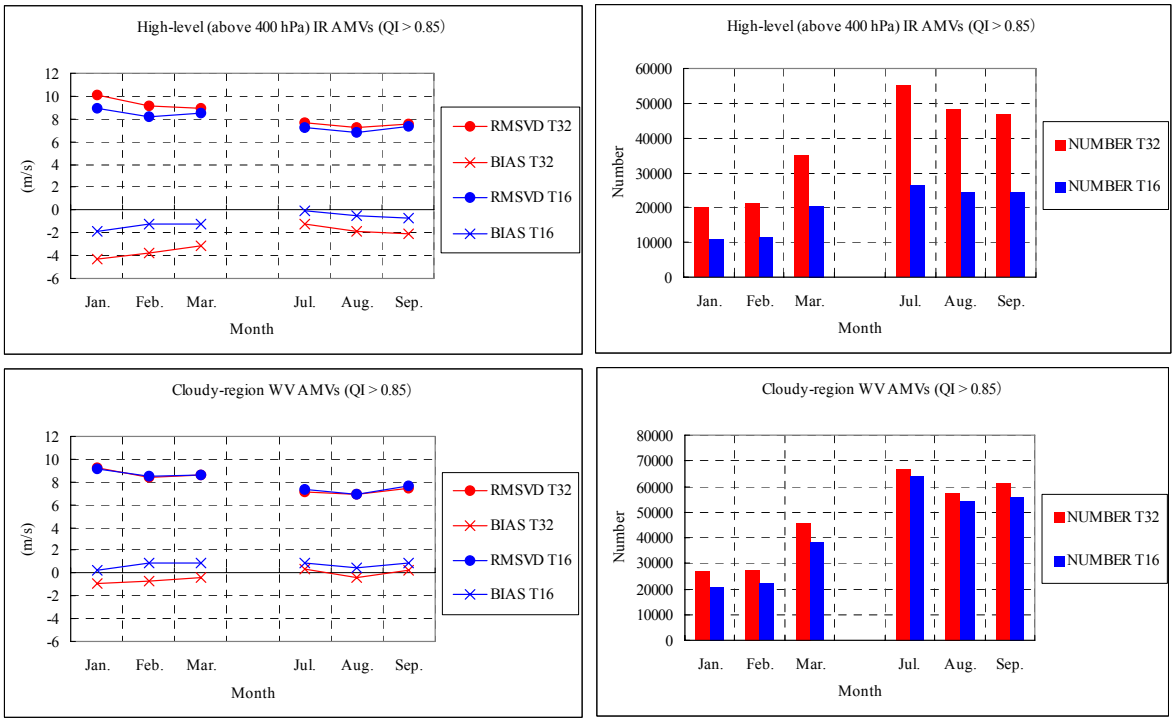

Figure 10: Monthly quality of high-level IR AMVs and cloudy-region WV AMVs (QI > 0.85) against sonde observations for common height assignment schemes (current schemes) and derivation area (20N-50N and 90E-170W within a satellite zenith angle of less than 60 degrees). The two kinds of AMVs are compared, those computed using a template image size of 16 (T16: Blue graphs) pixels and those using 32 (T32: Red graphs) pixels. The statistics are taken for AMVs computed for 2007.

With respect to IR AMVs for January 2009, as seen in Figure 11-1 (a) left, fast BIASes are observed in the previous AMVs at levels between 500 and 700 hPa for NH, SH and TR. As seen in Figure 11-2 (a), the fast BIAS problem is mitigated in the current AMVs. This improvement is mainly because the usage of CCij improves the height levels of previous AMVs which are erroneously assigned to lower height levels by the previous height assignment. In addition, the large slow wind speed BIASes beyond -3 m/s are found in the previous AMVs at levels between 100 and 500 hPa for NH in winter. The slow BIAS problem is also mitigated in the current AMVs. This improvement is due to resizing the template image as mentioned in Section 3.1. As for number, as seen in the comparison of Figure 11-1 (b) and 11-2 (b), the increase in the number of the current AMVs from previous AMVs for SH are larger at levels between 300 and 500 hPa compared to other height levels and regions. On the other hand, the numbers of the current AMVs for TR at levels between 200 and 300, and between 800 and 900 hPa are smaller than those of previous AMVs.

With respect to IR AMVs for July 2009, BIAS and number problems similar to January 2009 are found in the previous AMVs, specifically, the large fast bias between 500 and 700 hPa and slow bias between 100 and 500 hPa in winter hemispheres (i.e., SH) as seen in Figure 11-2 (a) left. Meanwhile, as seen in Figure 11-2 (a) right, both problems are improved or mitigated in the current AMVs. As for number, as seen in Figure 11-2 (b), the rates of increase of number of the current AMVs from previous AMVs for SH are larger at levels between 300 and 500 hPa and between 800 and 900 hPa. On the other hand, the number of the current AMVs is smaller for TR at levels between 200 and 300 hPa compared to that of previous AMVs.

Figure 12-1 and 12-2 show the same figures as Figure 11-1 and 11-2, but for cloudy-region WV AMVs. With respect to cloudy-region WV AMVs for January 2009, as seen in Figure 12-1, slow BIASes can be identified in the previous AMVs for NH as well as high-level IR AMVs. The slow BIAS problem is mitigated in the current AMVs. However, the fast BIASes at levels between 200 and 400 hPa in the current AMVs are slightly larger than those in the previous AMVs. These results are consistent with those obtained in the monthly statistics against sonde observations in Section 3.1.

With respect to cloudy-region WV AMVs for July 2009, as seen in Figure 12-2, the fast BIAS of the current AMVs has slightly increased from the previous AMVs as well as January 2009. One item of importance regarding the number is the increase of the current AMVs from the previous AMVs at levels between 300 and 400 hPa for NH and SH.

3.2.2 Spatial Dependency

In this section, the qualities of previous and current AMVs are investigated in terms of spatial dependency on JMA's GSM first-guess fields.

Figure 13-1 shows the spatial distributions of wind speed bias (BIAS) to GSM first-guess fields and number for the previous and current high-level (above 400 hPa) IR AMVs (QI > 0.85). Because of the expansion of the AMV derivation area since the upgrade, the current AMVs are computed over a region with higher Northern and Southern latitudes than the previous AMVs. Slow BIASes found between 20N and 50N in winter are overall smaller in the current AMVs than the previous AMVs while the density of the current AMVs is slightly less than that of previous AMVs in the entire computation area.

Figure 13-2 is the same figure for high-level IR AMVs as Figure 13-1, but for July 2009. The differences in the AMV derivation area and the data density between the previous and current AMVs have been identified as of January 2009. With respect to BIAS, slow BIASes are seen in the previous and current AMVs between 50S and

(a)

(b)

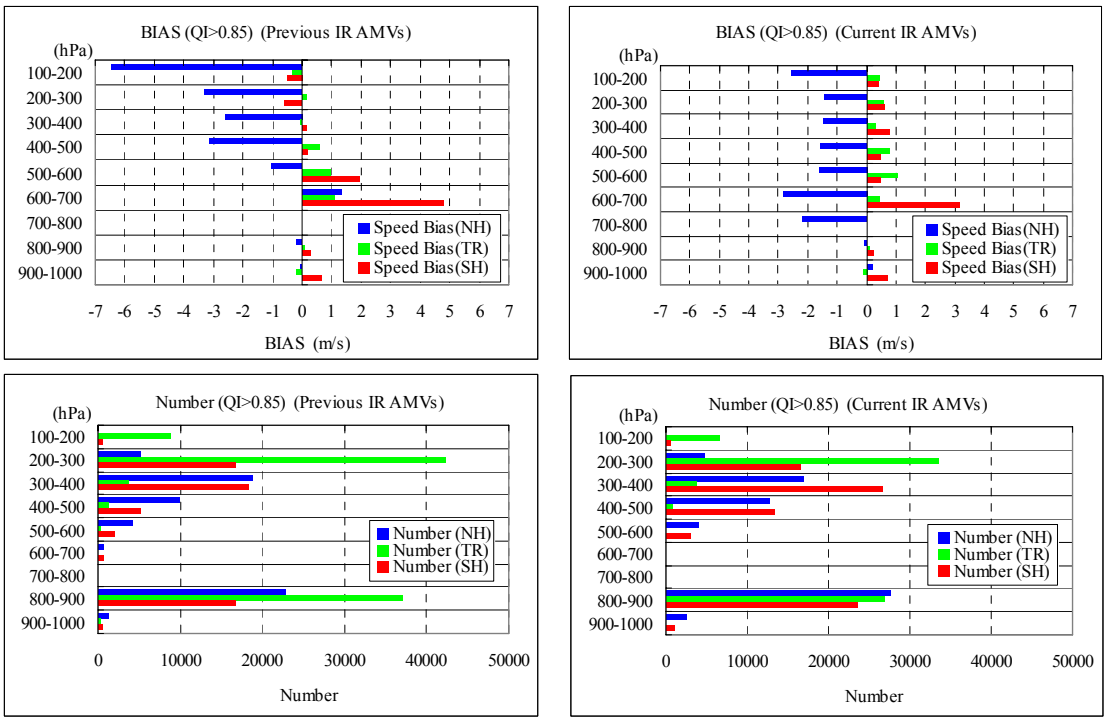

Figure 11-1: Height dependency of (a) wind speed bias against JMA's NWP first guess and (b) number of previous (left) and current (right) IR AMVs (QI > 0.85). The statistics are taken for AMVs computed for January 2009.

(a)

(b)

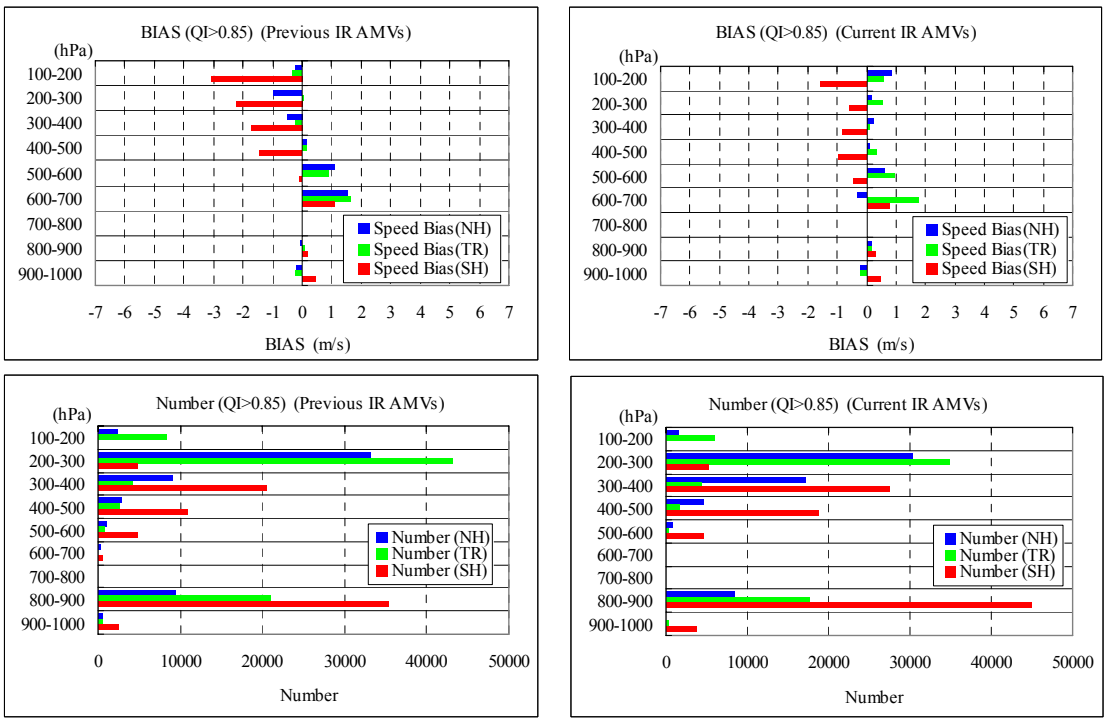

Figure 11-2: Same figure as Figure 11-1 for IR AMVs, but for July 2009.

(a)

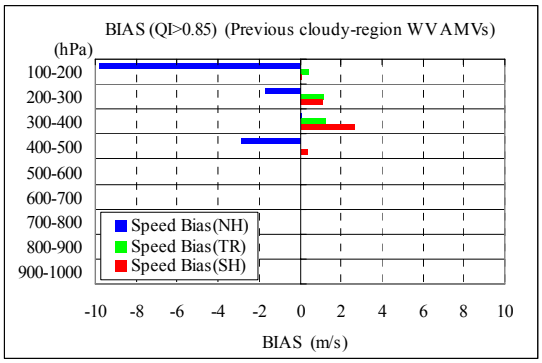

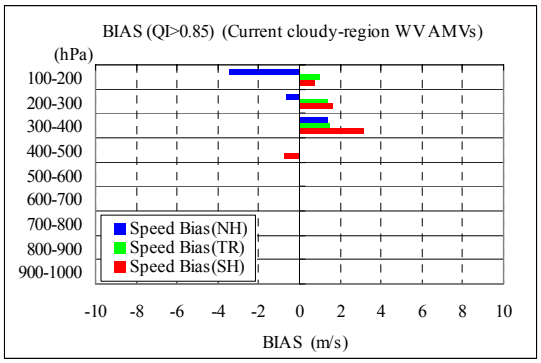

(b)

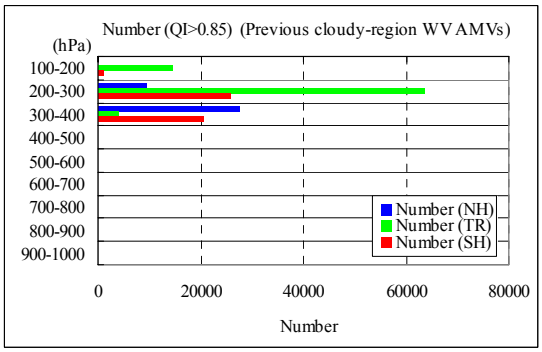

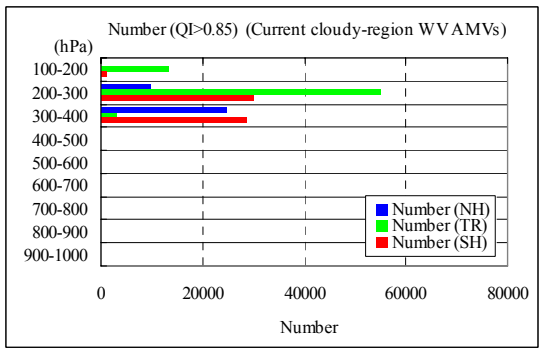

Figure 12-1: Height dependency of (a) wind speed bias against JMA's NWP first guess and (b) number of previous (left) and current (right) cloudy-region WV AMVs (QI > 0.85). The statistics are taken for AMVs computed for January 2009.

(a)

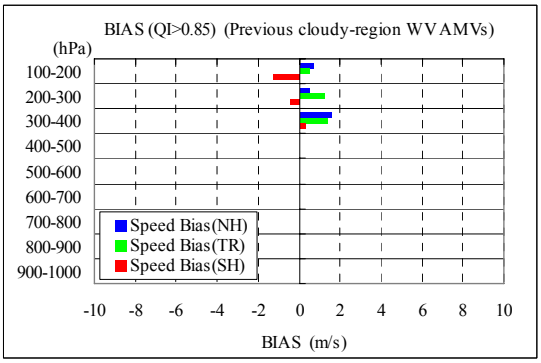

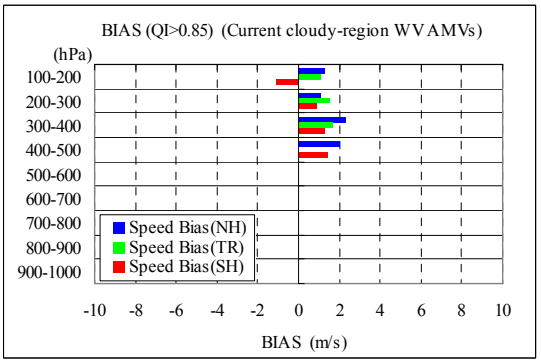

(b)

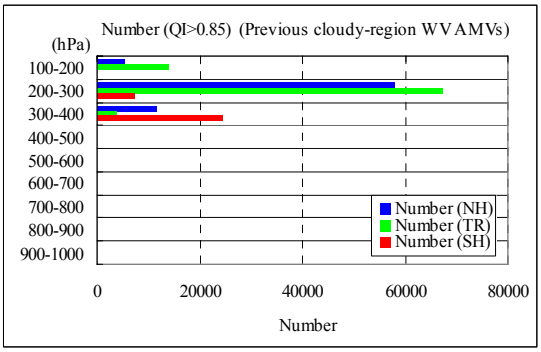

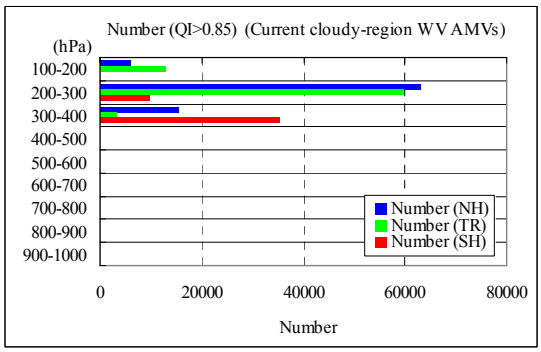

Figure 12-2: Same figure as Figure 12-1 for cloudy-region WV AMVs, but for July 2009.

20N in winter. However, the slow BIAS of the current AMVs is smaller than that of previous AMVs as of January 2009.

Figure 14-1 shows the spatial distributions of BIAS to GSM first-guess fields and number for the previous and current cloudy-region WV AMVs (QI > 0.85). Compared to the high-level IR AMVs for January 2009 shown in Figure 13-1, the difference of data density between the previous and current AMVs is smaller over the entire computation area. With respect to the BIAS, the slow BIASes of the previous AMVs over the region between 20N and 50N in winter are slightly mitigated in the current AMVs, while the fast BIASes slightly increase in the current AMVs at some locations in high and middle latitudes.

Figure 14-2 shows the same figure for cloudy-region WV AMVs as Figure 14-1, but for July 2009. The slow BIASes of the previous AMVs over the region between 60S and 20S in winter are slightly mitigated in the current AMVs, while the fast BIASes slightly increase in the current AMVs at some locations in high and middle latitudes. These situations are similar to those found in January 2009. The difference of data density between the previous and current AMVs for July 2009 is small, as is the case for January 2009.

4. Discussions and future plans

JMA/MSC will continue efforts to improve the quality of AMVs in the future. One important task is the revision of height assignment for low-level AMVs, i.e., abolishing the 850-hPa height limitation on AMV heights. The revision will contribute to expanding data availability in height.

Furthermore, the improvement of the fast speed bias identified for cloudy-region WV AMVs through the year is another future task. This problem is caused by the difficulty in using different channel images between feature tracking (by WV image) and height assignment (by IR image) due to the transparency of IR radiance and the opaqueness of WV radiance in water vapor layers. Figure 15 shows an illustration for two types of template images where clouds and water vapor layers coexist. As seen in Figure 15 (a), if a cloud (cloud1 in Figure 15 (a)) and a water vapor layer (WV1 in Figure 15 (a)) are at the same height level, the motion vector of the AMV derived using WV images is assigned to the consistent height level, the top of cloud1, which is derived using IR image. On the other hand, if a water vapor layer (WV2 in Figure 15 (b)) is above a cloud (cloud2 in Figure 15 (b)) as in Figure 15 (b), the height of the AMV is determined to be the top of cloud2 from IR images while the motion vector is derived by tracking the pattern of WV2 from WV images, leading to a disparity between feature tracking and height assignment. One way to mitigate the disparity problem is to improve the method of categorizing cloudy/clear-sky WV AMVs, i.e., it is thought that only template images like Figure 15 (a) should be regarded as such for cloudy-region WV AMVs.

JMA/MSC believes that the generation of its own cloud analysis product is an important long-term future task for upgrading the AMV derivation technique. This product is expected to improve not only the fast bias of cloudy-region WV AMVs, but also overall schemes for target selection and height assignment.

Acknowledgement

The author appreciates the valuable comments from Mr. Takanori Matsumoto, Mr. Kazuki Shimoji and Mr. Arata Okuyama of JMA/MSC, and the valuable proposals from the referee for this article.

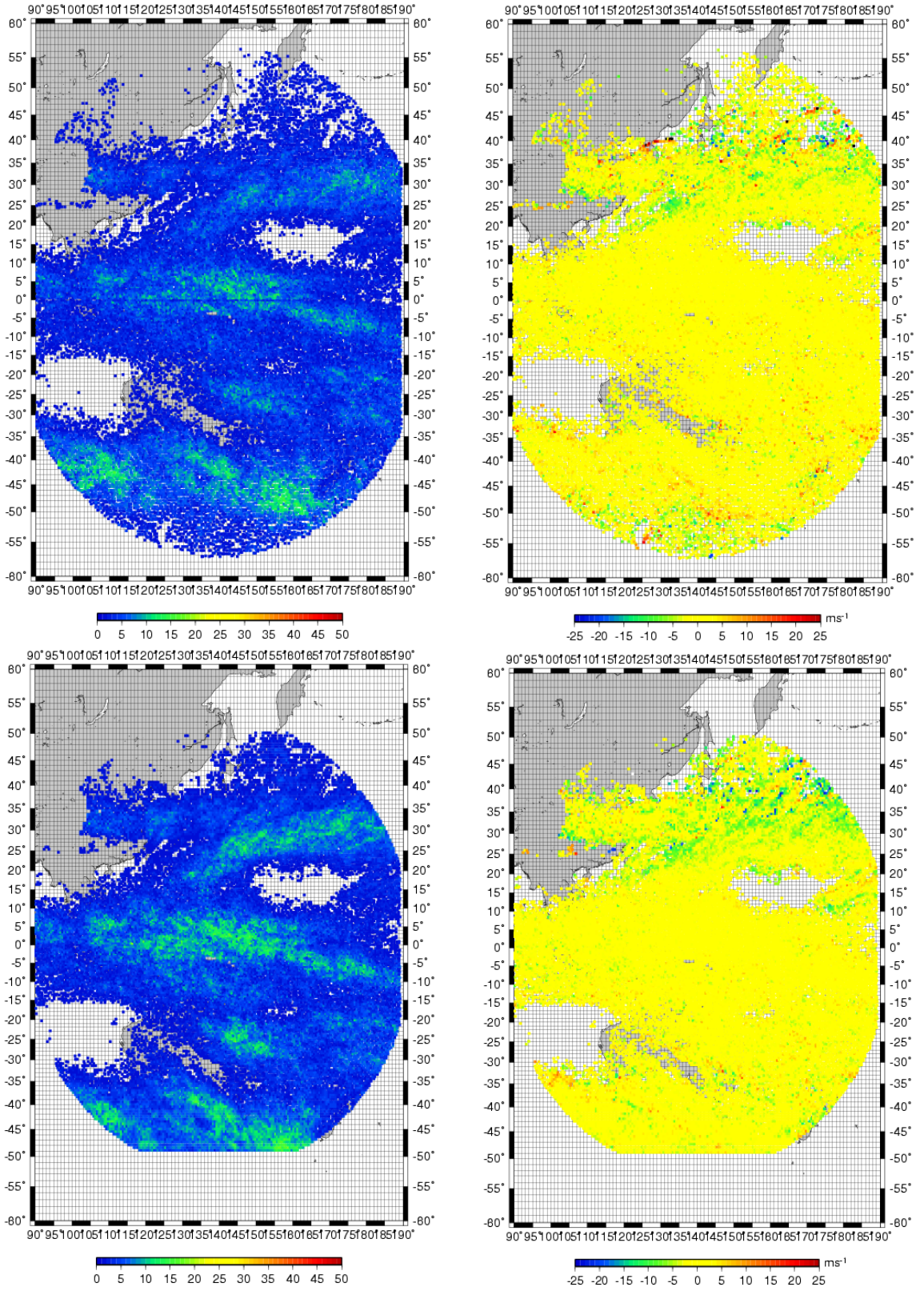

Figure 13-1: Number (Left) and wind speed bias (Right) against JMA's GSM first-guess fields on 0.5 degree latitude/longitude grids for high-level (above 400 hPa) IR AMVs (QI > 0.85). Upper: current AMVs, bottom: previous AMVs. The statistics are taken from AMVs computed for January 2009.

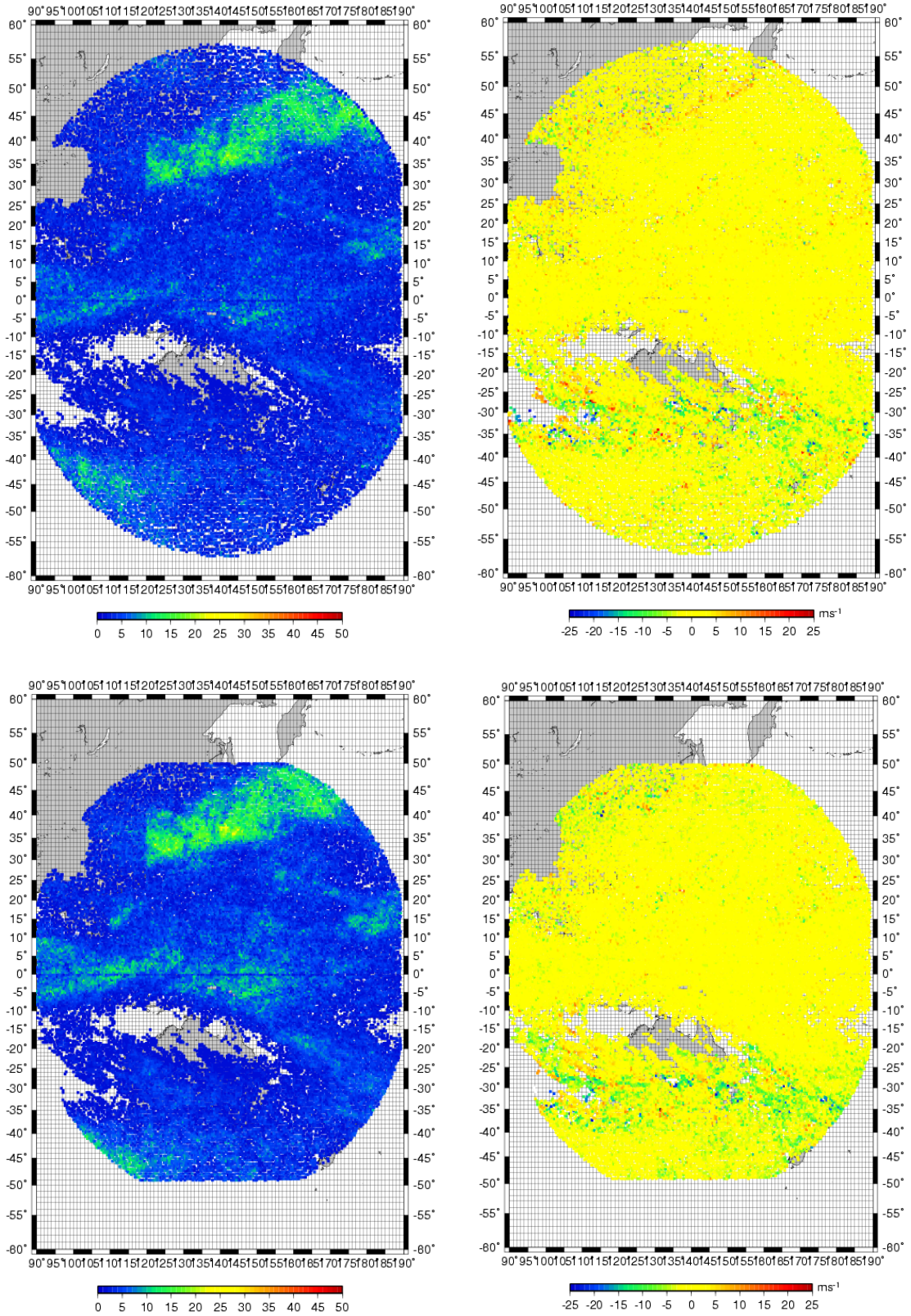

Figure 13-2: Same figure as Figure 13-1 for high-level IR AMVs, but for July 2009.

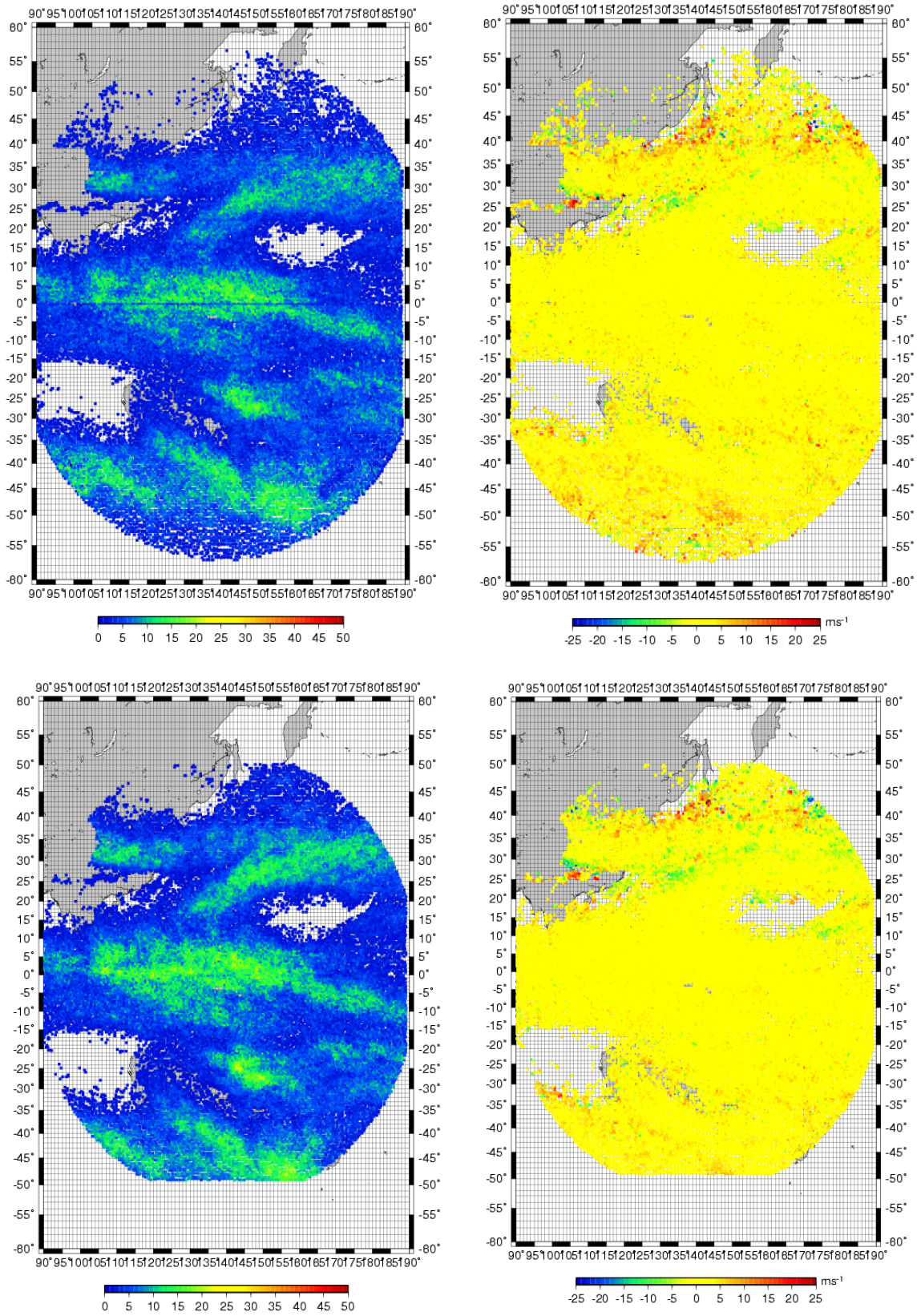

Figure 14-1:　Number (Left) and wind speed bias (Right) against JMA's GSM first-guess fields on 0.5 degree latitude/longitude grids for cloudy-region WV AMVs (QI > 0.85).　Upper: current AMVs, bottom: previous AMVs.　The statistics are taken from AMVs computed for January 2009.

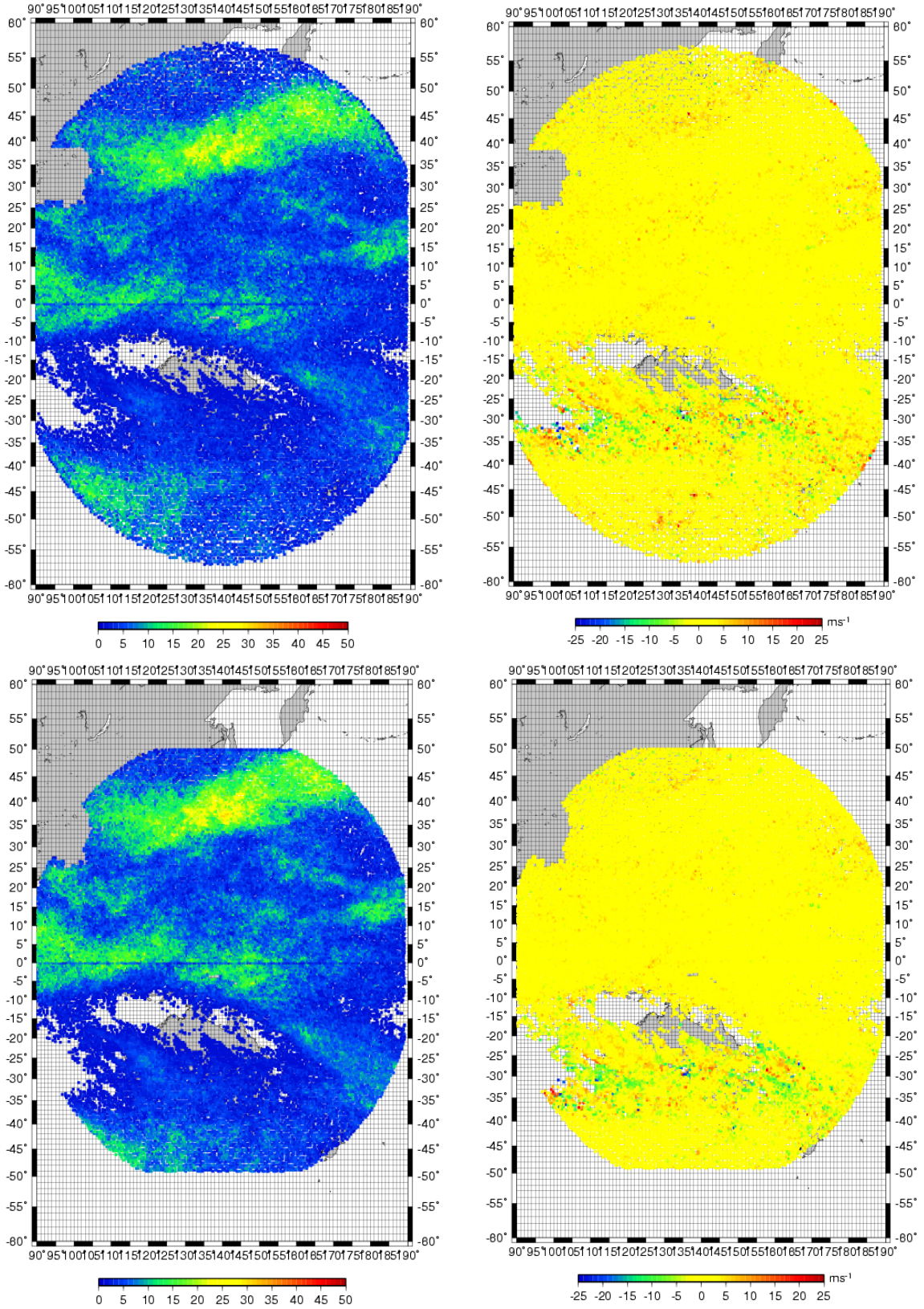

Figure 14-2: Same figure as Figure 14-1 for cloudy-region WV AMVs, but for July 2009.

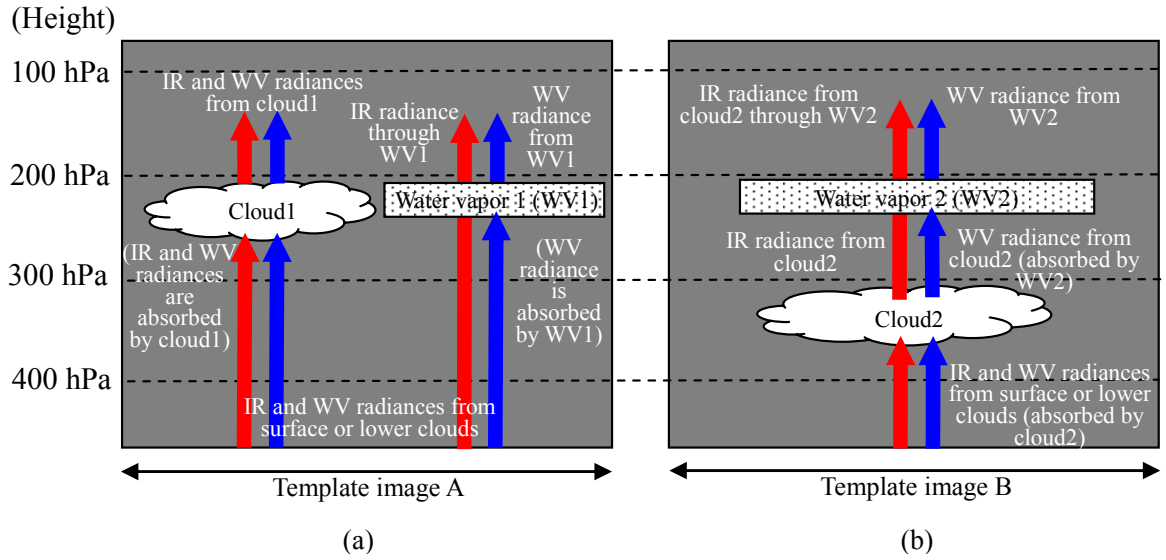

Figure 15: Illustration for two types of template images where cloud and water vapor layer coexist. Red and Blue arrows represent IR (10.8 micrometer) and WV (6.8 micrometer) radiances, respectively.
(a) A cloud (black body density) and a water vapor layer at the same height level.
(b) A water vapor layer above a cloud.

References

Büche, G., H. Karbstein, A. Kummer, and H. Fischer, 2006: Water vapor structure displacements from cloud-free METEOSAT scenes and their interpretation for the wind field, J. Appl. Meteor., 45, 556–575.

Hamada, T., 1979: Cloud wind estimation system, Meteorological Satellite Center technical note, Summary of GMS system, special issue II-2, 15–42 (in Japanese).

Holmlund, K., 1998: The utilization of statistical properties of satellite-derived atmospheric motion vectors to derive quality indicators, Weather and Forecasting, 13, 1093–1104.

Imai, T. and R. Oyama, 2008: Developments for quality improvement of Atmospheric Motion Vectors product, Meteorological Satellite Center technical note, 51, 41–55 (in Japanese).

JMA, 2007: JMA's Atmospheric Motion Vectors, JMA-WP-06, CGMS35.

JMA, 2009: JMA's Atmospheric Motion Vectors, JMA-WP-05, CGMS37.

JMA/MSC, 1980: The GMS Users Guide, 36–42, Meteorological Satellite Center.

Nieman, N. J., Schmetz and W.P. Menzel, 1993: A comparison of several techniques to assign heights to cloud tracers, J. Appl. Meteorol., 32, 1559–1568.

Ohkawara, N., T. Imai and R. Kumabe, 2004: Developing the high-density Atmospheric Motion Vector product, Meteorological Satellite Center technical note, 45, 1–16 (in Japanese).

Olander, Timothy L., 2001: UW-CIMSS Satellite-derived Wind Algorithm User's guide.

Onogi, K., J. Tsutsui, H. Koide, M. Sakamoto, S. Kobayashi, H. Hatsushika, T. Matsumoto, N. Yamazaki, H. Kamahori, K. Takahashi, S. Kadokura, K. Wada, K. Kato, R. Oyama, T. Ose, N. Mannoji and R. Taira, 2007 : The JRA-25 Reanalysis. J. Meteor. Soc. Japan, 85, 369–432.

Oyama, R., R. Borde, J. Schmetz and T. Kurino, 2008: Development of AMV height assignment directly linked to feature tracking at JMA, Proceedings of the Ninth International Winds Workshop, U.S.A.

Oyama, R. and K. Shimoji, 2008: Status of and future plans for JMA's Atmospheric motion vectors, Proceedings of the Ninth International Winds Workshop, U.S.A.

Schmetz, J., K. Holmlund, J. Hoffman, B. Strauss, B. Mason, V. Gartner, A. Koch, and L. van de Berg, 1993, Operational cloud-motion winds from Meteosat infrared images. J. Appl. Meteor., 32, 1206–1225.

Sohn, E. and R. Borde, 2008: The impact of window size on AMV, Proceedings of the Ninth International Winds Workshop, U.S.A.

Tokuno, M., 1998: Improvements in the method to extract operational cloud motion winds and water vapor motion winds of the GMS-5 system, Proceedings of the Fourth International Winds Workshop, 61–68, Switzerland.

Uchida, H. and S. Takata, 1996: Cloud and water vapor motion winds, Summary of the GMS-5 system, Meteorological Satellite Center technical note special issue, 103–110 (in Japanese).

Xu, J., Q. Zhang, F. Xiang, L. Jian, 1998: Cloud motion winds from FY-2 and GMS-5 meteorological satellites, Proceedings of the Fourth International Winds Workshop, 41–48.

大気追跡風算出アルゴリズムのアップグレードについて

小山 亮

要　旨

気象衛星センターでは、1978 年以降、静止気象衛星の連続する複数の画像を使用して大気追跡風(AMV)を算出している。現在は、MTSAT-1R の赤外(IR: 10.8μm)、水蒸気(WV: 6.8μm)、可視(VIS: 0.63μm) および短波長赤外(SWIR: 3.8μm)画像から、それぞれ IR AMV(赤外風)、WV AMV(水蒸気風)、VIS AMV(可視風)および SWIR AMV(短波長赤外風)を算出している。算出したデータは、重要な風データとして、気象庁および国外の数値予報センターで数値予報モデルための同化データとして利用されている。

本技術報告では、2009 年 5 月 19 日 05UTC に実施した大気追跡風のアップグレードの概要とともに、最新の大気追跡風算出アルゴリズムを総括的に記述する。本アップグレードにおける改良点は３つである。まず、上中層 IR AMV の高度指定法を雲域の追跡処理とリンクさせた手法にアップグレードしたことによって、アップグレード前の IR AMV にみられた高度指定誤差に起因する対流圏中層の正バイアスの改善、及び上層での算出数減少が改善された。二つ目に、雲または水蒸気パターンの追跡に使用する画像小領域のサイズの見直しによって、特に冬半球中高緯度域の上層 IR AMV と WV AMV でみられる負の風速バイアスが従来の AMV に比べて軽減された。三つ目に、大気追跡風の算出範囲を 50S-50N 及び 90E-170W の領域から 60S-60N 及び 90E-170W に拡張を行うことで、従来に比べてより高緯度域のデータがユーザーへ提供されるようになった。現在の算出アルゴリズムは、現在実施中である GMS-1、3、4 及び 5 号、GOES-9 及び MTSAT-1R のデータを使用した大気追跡風の再処理にも使用されている。再処理した大気追跡風データは、2009 年から 2012 年にかけて計画されている JRA-55 長期再解析および SCOPE-CM(気候監視のための環境衛星データ処理に関する調整会議)へ提供される予定である。